Department of Physics and Astronomy

Heidelberg University

Master thesis

in Physics

submitted by

Paula Herrero Gascón

born in Valencia, Spain

2022

Study of potential decay-time biases in the data processing of the upgraded LHCb experiment

This Master thesis has been carried out by Paula Herrero Gascón

at the

Physikalisches Institut

under the supervision of

Prof. Dr. Stephanie Hansmann-Menzemer

and

Dr. Peilian Li

Kurzfassung

Das Upgrade des LHCb Experiments wird im Frühjahr 2022 anfangen bei einer instantanen Luminosität von bis zu $2 \times 10^{33}\text{cm}^{-2}\text{s}^{-1}$ Daten aufzunehmen. Der verbesserte Detektor kann bei einer Proton-Proton Kollisionsrate von 40 MHz ausgelesen werden. Um Kollisionsereignisse, die interessante b- und c-Quarks und deren Hadronen enthalten bei so hohen Raten effizient zu selektieren, wird ein rein software-basiertes Triggersystem benötigt. Dafür wurde neben der Erneuerung verschiedener Subdetektoren die gesamte Rekonstruktionssoftware inklusive der Algorithmen neu implementiert und optimitiert. Da es sich um ein neues System handelt, ist es essentiell seine Leistungsfähigkeit in Bezug auf die Untersuchung physikalischer Prozesse zu validieren. Die exakte Rekonstruktion der Zerfallszeiten von b-Hadronen ist entscheidend für Messungen zeitabhängiger physikalischer Größen mit LHCb. In dieser Arbeit wird der Einfluss der Datenverarbeitung auf die Zerfallszeitenverteilung von simulierten $B^+ \to J/\psi\ K^+$ und $B^0 \to J/\psi\ K^{*0}$ Zerfällen untersucht. Die Rekonstruktion der Zerfallszeiten wird erläutert und mit den wahren Werten aus der Simulation verglichen. Die durchschnittliche Auflösung der Zerfallszeit beträgt 0.032 ps. Es wurde kein signifikanter, durch die Rekonstruktion verursachter Bias der Zerfallszeit beobachtet.

Abstract

The upgraded LHCb experiment will start data taking in spring 2022 with an instantaneous luminosity of up to $2 \times 10^{33}\text{cm}^{-2}\text{s}^{-1}$. The upgraded detector is designed to be read out at the LHC bunch crossing rate of 40 MHz. To effectively select the interesting events containing b and c hadrons at such high rates, a pure software-based trigger system is required. Apart from the replacement of different subdetectors, the entire reconstruction framework and its algorithms have been reimplemented and optimized. To be well-prepared for the data taking, it is essential to validate the physics performance of this new detector and its software. The precise reconstruction of the decay time of b hadrons is vital for many time-dependent physics measurements at LHCb. In this thesis, the effects of the data processing on the decay-time distribution are studied using simulated samples of $B^+ \to J/\psi\ K^+$ and $B^0 \to J/\psi\ K^{*0}$ decays. The performance of the reconstructed decay times is also evaluated comparing to results obtained with simulated values. An average resolution of the reconstructed values of 0.032 ps is obtained. No significant reconstruction-induced bias is found, indicating a good performance of the reconstruction in terms of the decay time for the LHCb upgrade.

Contents

1 Introduction

The definition of physics (from the Greek *physikos*) is the science concerned with all aspects of nature on both the macroscopic and submicroscopic levels [1]. This naturally states the importance of the Particle Physics discipline which is concerned with the fundamental constituents of the Universe and the interactions between them. All the knowledge in this field acquired during the last centuries is embodied in the Standard Model (SM) of particle physics. This extensive model successfully describes most of the experimental observations in particle physics. It also predicted the existence of the Higgs boson, the last missing particle of the SM, which was observed for the first time in 2012 at the Large Hadron Collider (LHC) [2][3].

Despite the success of the SM describing the elementary particles, there are important phenomena of the universe that can not be explained with this model. Examples are the force of gravity, which is not included in the model, the existence of dark matter, or the non-zero neutrino mass. One of the most powerful tools available nowadays to broaden the knowledge of particle physics is the LHC. The LHCb experiment, located in one of the four interaction points of the LHC, is dedicated to the detection and study of decays of hadrons containing heavy quarks. Until 2018, the LHCb experiment has acquired a great amount of data whose analysis advanced the understanding of particle physics and revealed some interesting tensions which might hint to physics phenomena beyond the SM, so-called New Physics (NP) [4] [5]. To further test these tensions it is important to obtain results with higher precision than the SM calculations. Thus additional data is needed to improve the statistical sensitivity of the measurements. Therefore the LHCb experiment is currently being upgraded, to be able to handle a five times higher instantaneous luminosity[1] than before. The new data taking period is expected to start in Spring 2022.

This upgrade involves important changes in the detector and the trigger strategy of the experiment. Several subdetectors are completely replaced to achieve higher granularity and radiation hardness for the increased luminosity. In addition, the old hardware trigger is removed, and a full software trigger strategy is adopted. The new trigger model is designed to be completely executed in real time with reconstruction quality comparable to offline processes. In addition, there are different streams for the persistency of the events which depended on the trigger line requirements. Around 70% of events will be stored through the TURBO persistence model, which only saves the information related with the signal candidate. The impossibility of accessing the whole event information in a later stage of the analysis and the

[1] Luminosity ($\mathcal{L}$) is the ratio of the number of events detected ($\mathrm{d}N$) in a certain period of time ($\mathrm{d}t$) to the cross-section (σ), which in the case of the LHC corresponds to cross-section of protons or heavy ion collisions, $\mathcal{L} = \frac{1}{\sigma}\frac{\mathrm{d}N}{\mathrm{d}t}$.

reconstruction algorithms developed for the new trigger strategy, require a precise validation of their physics performance before the data taking period starts.

The study presented in this thesis forms part of this evaluation. The study consists in the search of a possible decay-time bias introduced in the data processing from the track reconstruction to the final trigger decisions. In the processing of the data a time bias is introduced when an efficiency is not constant in the full decay time range, thus the time distributions are affected. The evaluation of the decay time reconstruction by the new detector and software is a key step in the preparation for future analyses because lifetime and time-dependent measurements form a big part of the physics programme by the LHCb experiment. These include measurements of the lifetimes of several b hadrons and the time-dependent measurements necessary for analyses of oscillating systems.

The study is performed on $B^+ \to J/\psi\, K^+$ and $B^0 \to J/\psi\, K^{*0}$ signal candidates on simulated data. The effect of each reconstruction step on the decay-time distribution of the b hadrons is evaluated by performing a fit of the B lifetime. Changes in the obtained lifetime, imply the introduction of a time bias by a specific reconstruction step. The whole processing of the data is investigated, from the individual stable particles reconstruction, the combining to decaying particles, to the selection stage. Firstly, the dependence of the efficiency of each step on the decay time of the b hadron is studied. Secondly, the resolution of the reconstruction of the decay-time values is evaluated.

In the following chapters, first, a theoretical introduction to the SM is given. The second chapter consists in a detailed description of the LHCb experiment. The third chapter motivates the study and gives the necessary tools for a lifetime measurement. The results are presented in Chapter 4, where firstly, the time-dependent acceptance is studied step by step and secondly the reconstructed decay times are analysed. Finally, in Chapter 5 the conclusions are presented and possible improvements of the study are mentioned.

2 The Standard Model

The Standard Model (SM) [6] is the theory used nowadays to describe the known elementary particles and their interactions. In the SM, particles are represented by a quantized quantum field, with which it is capable to explain three of the four forces present in nature, i.e. the electromagnetic, the weak, and the strong interaction. The fourth one is the gravitational force, and the way to combine it with the SM theory is still a line of research.

The SM classifies the elementary particles in fermions, which form the known matter, the gauge bosons, which are in charge of the mentioned interactions, and the last discovered particle, the Higgs boson [2][3]. The fermions are divided into quarks and leptons, and both groups are again divided into three generations. The first generation of quarks contains the lightest ones, the up u and down d quarks. The second generation is formed by the charm c and strange s quarks, and the third generation contains the heaviest quarks, the top t and bottom b quarks. Quarks carry electromagnetic charge as well as colour charge, therefore they interact through the electromagnetic, the weak, and the strong force. The leptons are three doublets and are also ordered by mass in three generations. They are the electron e, the muon μ, and the tau lepton τ, which carry electromagnetic charge, and their corresponding neutrinos. The fermions just interact via electromagnetic (except neutrinos) and weak forces, because they do not carry colour charge. The masses and the charges of these particles are presented in Fig. 2.1. The gauge boson described in the SM: the photon γ is massless and responsible for the electromagnetic interaction, the eight gluons are in charge of the strong interaction, and the $W^{\pm}$ and Z bosons are in charge of the weak interaction.

Quarks are not naturally found individually. Instead, they are bound by gluons with the strong force in composite particles, which are called hadrons. There exist hadrons with a different number of quarks: mesons that contain two quarks of opposite colour charges, baryons that have three quarks, and rarer particles like tetraquarks [8] and pentaquarks [9]. For the study performed in this thesis, the decays of B mesons, in which one of the two quarks is of type b, have been used.

B mesons are especially interesting for several reasons. Firstly, the b quark is the heaviest quark that hadronizes, because the more massive top quark decays before hadronizing. Therefore, B mesons have a broader spectrum of decay channels than

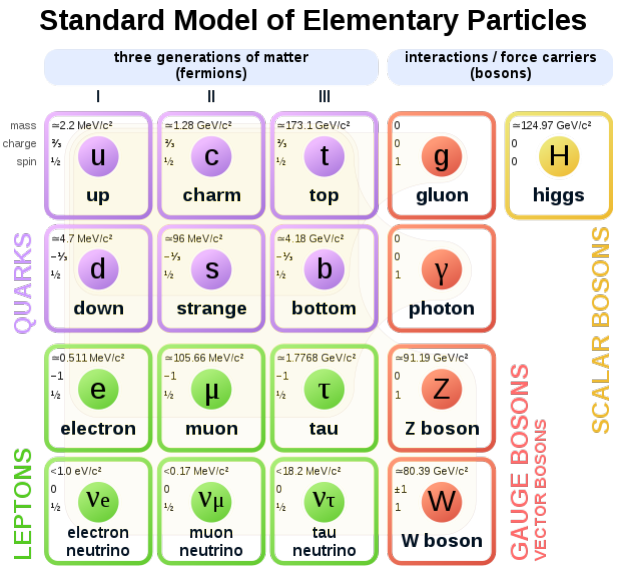

Figure 2.1: The matter content of the Standard Model. Source: Wikipedia.

other mesons. Secondly, they only decay weakly[1], which results in longer lifetimes that make them easier to be distinguished from other particles inside a detector.

When a B meson decays weakly, for example, the decay shown in Fig. 2.2, the state of the b quark that forms the meson and interacts with the W boson is not the mass eigenstates. The b quark that interacts with the W boson is in a weak eigenstate. The weak eigenstates are a combination of the three mass eigenstates. The coefficients that relate the weak and the mass eigenstates are known as the

[1]Excited states of B mesons can decay electromagnetically or via strong interaction to a ground state, but eventually they will decay weakly to undergo a flavour transition, only permitted via the weak interaction.

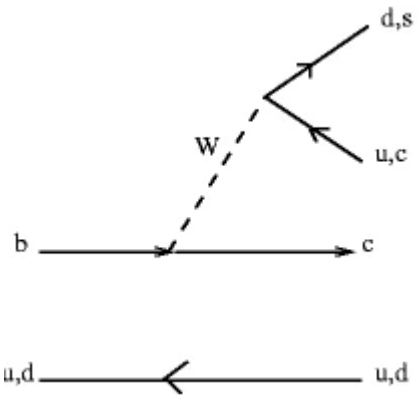

Figure 2.2: Feynman diagram of a generic hadronic decay of a b-hadron. Source: [7].

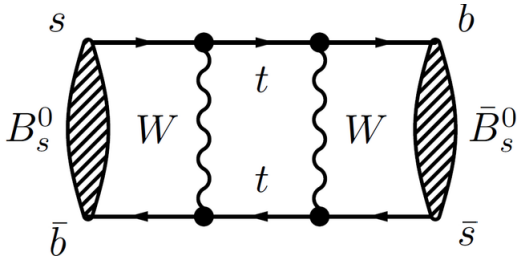

Figure 2.3: Box diagram of the $B_s^0 - \overline{B}_s^0$ system. Source: Wikipedia.

Cabibbo–Kobayashi–Maskawa (CKM) matrix:

$$\begin{bmatrix} d' \\ s' \\ b' \end{bmatrix} = \begin{bmatrix} V_{ud} & V_{us} & V_{ub} \\ V_{cd} & V_{cs} & V_{cb} \\ V_{td} & V_{ts} & V_{tb} \end{bmatrix} \begin{bmatrix} d \\ s \\ b \end{bmatrix},$$

where $q' = [d', s', b']$ denotes the weak interaction eigenstates and $q = [d, s, b]$ denotes the mass eigenstates. The elements of the CKM matrix are fundamental constants of the SM.

Another feature of the SM that involves the B mesons, are the oscillations of neutral mesons. This was first observed in the neutral kaon system [10]. This occurs for example via the diagram shown in Fig. 2.3 because the flavour eigenstates, $B_{(s)}^0$ (u or s and $\bar{b}$) and $\overline{B}_{(s)}^0$ ($\bar{u}$ or $\bar{s}$ and b), are not the same as the physical states, the mass eigenstates, that propagate in time.

The neutral mesons oscillation phenomenon can be affected by CP violation. The charge-parity symmetry (CP) is broken when the oscillation probability for the particle and antiparticle is not the same. This is the reason why these oscillating systems are a key tool in order to study the effect of the broken CP symmetry in the SM by measuring different physics observables.

3 The LHCb experiment

This chapter contains a detailed description of the LHCb experiment. In the first two sections, the Large Hadron Collider (LHC) and the LHCb experiment are outlined. The LHC started data taking in 2008. After two successful running periods (Run 1 from 2010 until 2012 and Run 2 from 2015 until 2018), the LHCb experiment is currently upgraded. This thesis focuses on the preparation of Run 3, thus the upgraded LHCb experiment and its components are described here. Finally, the software of the experiment, containing the trigger system and the different parts of the data processing chain are described.

3.1 The Large Hadron Collider

The Large Hadron Collider (LHC) [11] is the world's largest hadron collider. It is a circular collider, and it is operated by the European Organization for Nuclear Research (CERN) in Geneva, Switzerland. It consists of a 27 km ring of superconducting magnets and it is located 100 m underground. Inside, two high-energy particle beams travel close to the speed of light guided by a strong magnetic field. To form these beams, particles need to be pre-accelerated before being injected into the LHC. This is done by a series of pre-accelerators, as can be seen in Fig. 3.1. At the LHC, both protons and heavy ions are accelerated and collided.

Protons, are extracted from the ionization of hydrogen and first accelerated in the Linear Accelerator 4 (LINAC4). Then, they are further accelerated in a series of circular accelerators with increasing circumferences from 157 m to 7 km. Finally, in the Super Proton Synchrotron, they are accelerated to about 450 GeV before being fed to the LHC in two opposite directions. The LHC then accelerates protons up to 6.5 TeV.

Protons circulate around the ring in well-defined bunches. Each proton beam has 2808 bunches, and each bunch contains about 10^{11} protons. When entering the interaction point these bunches are 20 µm wide. At full luminosity, the LHC uses a crossing rate of 40 MHz which corresponds to 25 ns bunch spacing.

There are four interaction points in the LHC and in each of them one of the four major experiments, ATLAS, CMS, ALICE, and LHCb is located. ATLAS and CMS focus on the study of heavy particles produced centrally in pp collisions, while ALICE studies properties of the quark-gluon plasma from heavy-ion collisions. Finally, the LHCb experiment is a forward spectrometer focused on decays of light particles containing b and c quarks.

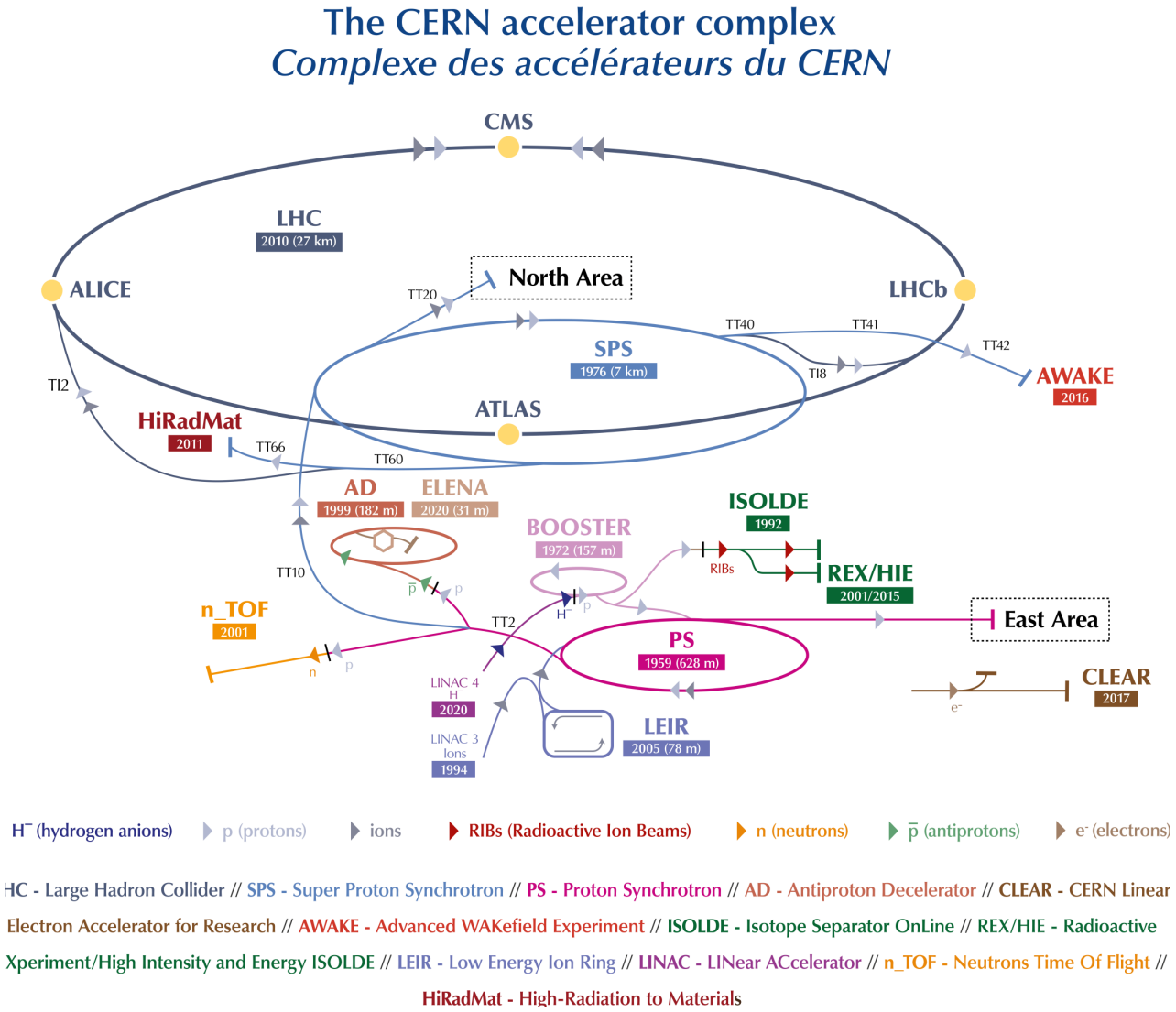

Figure 3.1: Layout of the accelerator complex at CERN. Source: cds.cern.ch.

3.2 The LHCb detector

The LHCb detector is a single arm forward spectrometer, unlike the other experiments at the LHC. ATLAS, CMS, and ALICE's detectors cover the full spatial angle due to their cylindric shape surrounding the collision point. In the LHCb experiment, the collision point is surrounded by the Vertex Locator, which is followed by the rest of the subdetectors stacked one behind the other as can be seen in Fig. 3.2. The forward design is optimized to study b decays, as the production of light $b\bar{b}$ pairs is maximal in the forward direction. Although the two protons that collide have the same energy, the actual collision happens at parton level. The main mechanism is gluon-gluon fusion. Due to the wide energy spectrum of the gluon inside the proton,

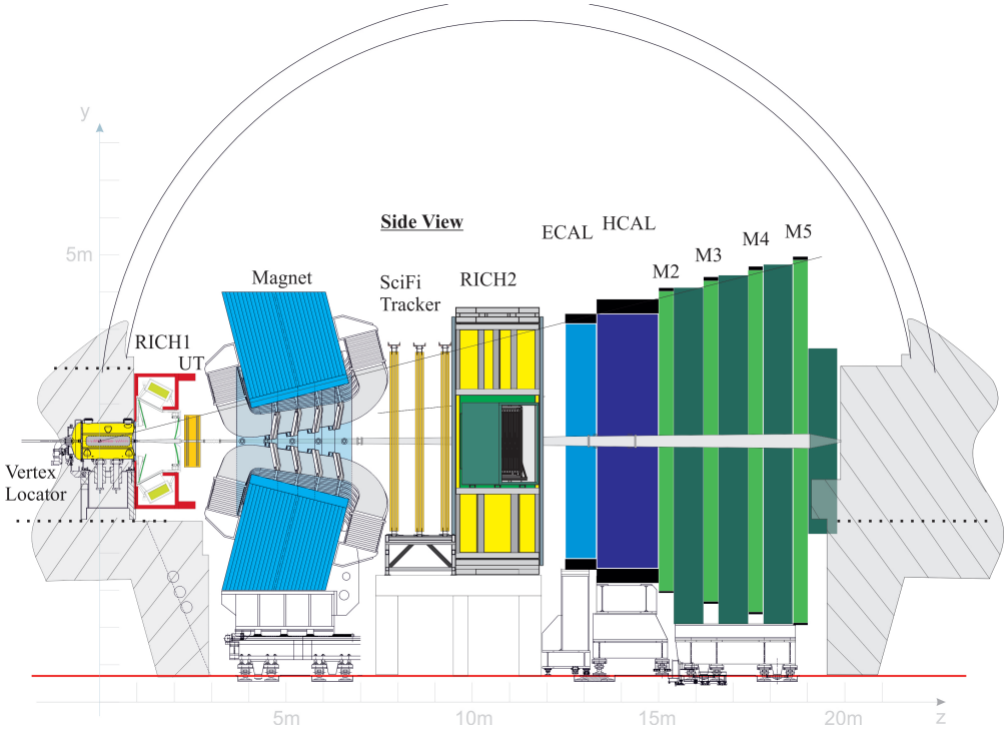

Figure 3.2: Outline of the side view of the LHCb Detector after the upgrade carried out during the Long Shutdown 2. Source: [12].

as can be seen in Fig. 3.3, the two gluons have different momenta and thus the $b\bar{b}$ pair is boosted either in the forward or backward direction.

The LHCb detector started taking data in 2010. It has remained mostly unmodified until the end of 2018 when Run 2 of LHC finished. During the first two runs of the LHC, the instantaneous luminosity was around 4×10^{32} cm^{-2} s^{-1} and the LHCb experiment acquired data corresponding to an integrated luminosity of 9/fb. At the moment, during the second Long Shutdown of the LHC (LS2), most of the subdetectors, as well as the trigger system, are upgraded in order to improve the performance of the LHCb experiment and prepare it for the next runs of the LHC with a higher instantaneous luminosity. In Run 3, the luminosity is planned to be 2×10^{33} cm^{-2} s^{-1}, five times higher than in Run 2. This implies an increase in the pileup of the detector. The number of collisions per bunch crossing will be between five and seven times higher than in Run 1 and 2. Thus a much higher density of particles inside the detector is expected and therefore the detector and the trigger system needed to be upgraded.

In the following, the new version of the detector and the trigger after the upgrade is described. The subdetectors of the LHCb experiment can be divided into two groups according to their function, the tracking system, and the particle identification system.

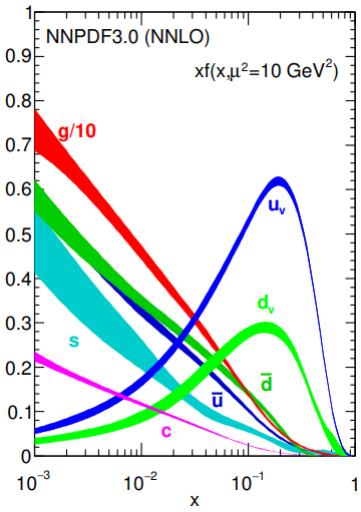

Figure 3.3: Distribution of the momentum of partons in the proton. f is the probability to find a parton at a given value, while x is the fraction of momentum of the proton carried by each parton. The plot illustrates $xf(x)$ as a function of x at a center of mass energy relevant for the LHC. The two peaked curves correspond to the valence quarks, which carry a higher momentum. At low energies there are the see quarks and the gluons. The gluons completely dominate in this energy range. To fit in one diagram the curve of the gluons is reduced by a factor of 10. The wide range of energies of the gluons is the reason for the angular distribution of $b\bar{b}$ pairs in the LHCb to be maximum in the beam direction. Source: [13].

3.2.1 Coordinate system

The LHCb detector is described using a right-handed Cartesian coordinate system. The origin is the interaction point. The z axis is set along the beam pipe with the positive direction pointing towards the end of the detector. The x axis is set horizontally pointing towards the centre of LHC and the y axis is set vertically upwards.

3.2.2 Tracking System

The purpose of this system is to reconstruct the trajectory of charged particles inside the detector, as well as their momenta, by the interaction of the particles with the different tracking stations. The tracking system consists of the Vertex Locator, the Upstream Tracker, the magnet, and the Scintillating Fiber Tracker.

Vertex Locator

The VErtex LOcator (VELO) [14] is the first subdetector and the one with the highest position resolution. It surrounds the interaction point, where the collision happens. Its main purpose is precise position reconstruction of particles close to the

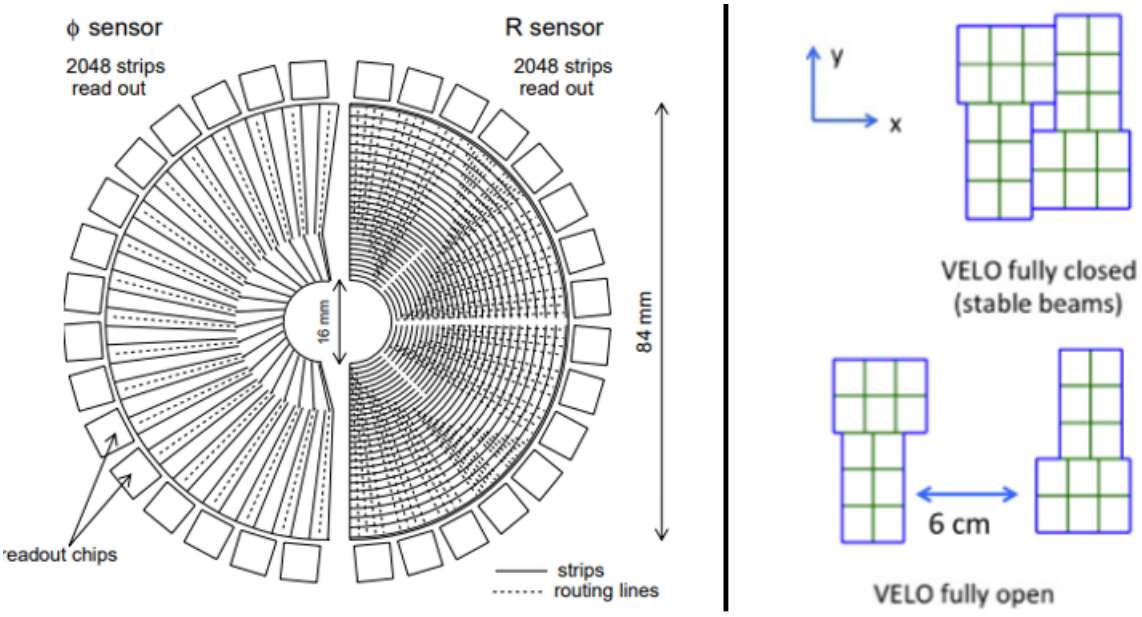

Figure 3.4: Comparison of the VELO modules used in Run 1 and Run 2 (left), in which the sensors are made of strips, and the ones used for the upgraded VELO, made with pixel sensors (right). Source: [14][15].

interaction point. It plays a key role in the vertex reconstruction. The VELO has been completely exchanged for the upgrade. The major differences with respect to the one used in Run 1 and Run 2 are highlighted here since it is the most involved subdetector in the study of this thesis.

To optimally profit from the five times higher luminosity the trigger system had to be modified. While in Run 1 and Run 2 a hardware trigger reduced the data rate from 40 MHz to readout rate of 1 MHz, in Run 3 the detector is read out at 40 MHz. Furthermore to cope with the higher instantaneous luminosity the former VELO strip detector was upgraded to a pixel detector. The VELO consists of 26 detector modules mounted orthogonally to the beam on each side. These are five sensors more than in Run 1 and Run 2. However, the most remarkable difference is the pixel sensors used for the new modules instead of strip sensors. In the old VELO, the strips were placed forming circles around the beam for the R sensors and in the radial direction for the Φ sensors. In the new version, the pixel modules look like in Fig. 3.4 (right). The completely different geometry of the old sensors and the new ones requires new reconstruction algorithms.

The distribution of the modules of the VELO along the z direction is not homogeneous, as can be seen in Fig 3.5. There is a higher density of modules close to the pp interaction point to ensure that enough sensors are hit by any particle originated in the collision. Also, in order to have a higher precision of the vertex position, the modules are only 5 mm away from the beamline, which is 2 mm closer than Run 1 and Run 2. The VELO is designed in two halves, so it can be opened during the

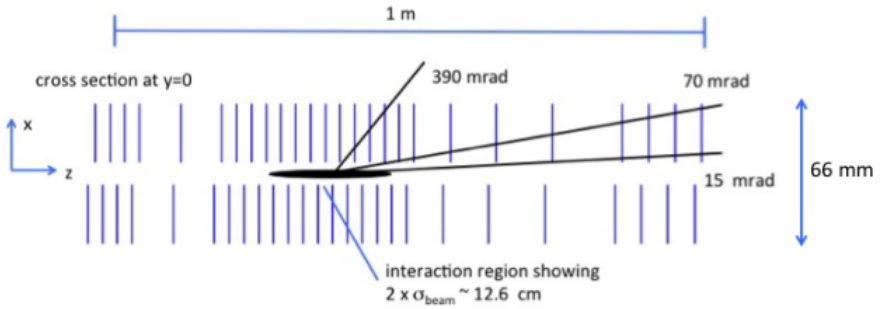

Figure 3.5: Distribution of VELO modules. These are placed to maximized the acceptance, hence higher density of modules in the interaction region. Source: [14].

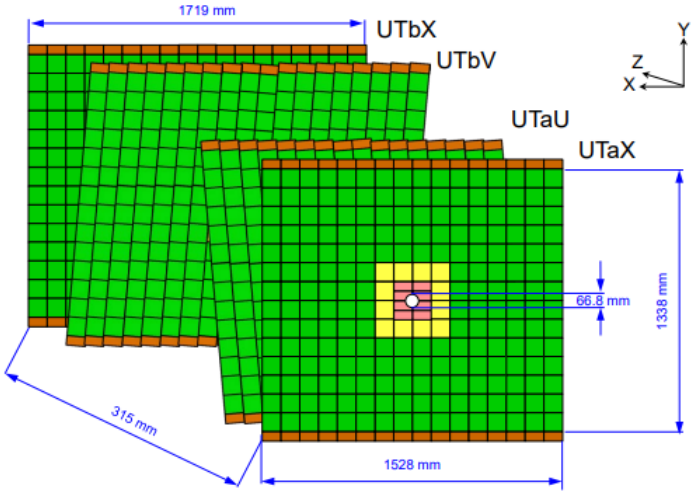

Figure 3.6: Outline of the Upstream Tracker. The different colours correspond to different sensors, with higher granularity in the center. Source: [12].

injection. Due to its closeness to the beam, it would not otherwise be safe during the beam injection. The last component of the VELO is a thin aluminium foil between the modules and the beam vacuum called RF-foil.

Upstream Tracker

The upstream tracker (UT) [12] is located after RICH 1 in the fringe field of the magnet. It takes part in the track reconstruction and in the momentum determination of the charged particles. It consists of four planes of silicon microstrips. To deal with the high occupancy in this part of the detector close to the collision point, the sensors closer to the beamline have a higher density of strips. The magnetic field curves the tracks in the horizontal plane ($x-z$ plane), thus the measurement of the x coordinate is particularly important. Therefore the strips are in vertical position and in order to obtain the y coordinate information, the two inner planes are tilted 5° degrees in the $x-y$ plane. This geometry can be better understood with Fig 3.6.

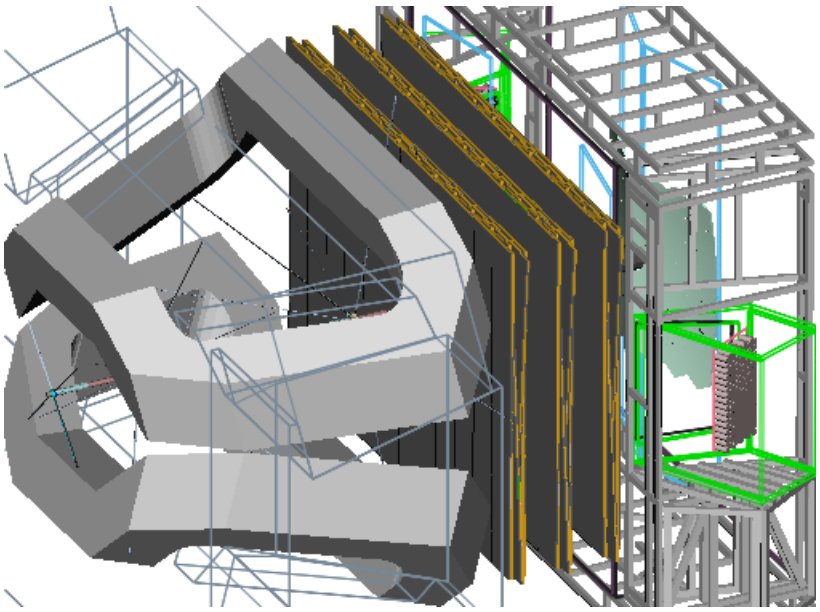

Figure 3.7: Sketch of the position of the SciFi. It is located after the magnet and before the RICH2. Source: [12].

Magnet

After the UT, there is the magnet. It is a dipole magnet made of two big coils and produces an integrated magnetic field of 4 Tm. Its purpose is to bend the particles according to Lorentz force and allow for momentum estimation by measuring the curvature radius. The main component of the magnetic field is in the y direction; therefore, the tracks of charged particles are curved in the horizontal plane in opposite directions for opposite charges. In order to avoid asymmetries in the reconstruction due to differences in the performance of the right part of the detector in comparison with the left part, the polarity of the magnet is switched during data taking and both datasets are later combined.

Scintillating Fiber Tracker

The Scintillating Fiber (SciFi) [12] Tracker is the subdetector located after the magnet and the one in charge of reconstructing the trajectories of the charged particles. Together with the particle slope measured in the VELO before the magnet, the momentum of the particles can be inferred. The SciFi Tracker consists of three tracking stations each with four detection planes. In these planes, the scintillating fibers are placed, mostly in the y direction for a precise x measurement. To also have some y-coordinate information, similar as in the UT, the two inner planes are tilted $\pm 5°$ from the vertical. A closer image of the SciFi Tracker is represented in Fig. 3.7.

Each of the planes has twelve SciFi modules. These modules are 5 m long and in both of its ends, upper and lower, the Silicon PhotoMultipliers (SiPMs) are located.

The SiPMs are in charge of detecting the photons produced by the interaction of the charged particles with the scintillating fibers.

3.2.3 Particle Identification system

The Particle Identification system is the other group of subdetectors. The goal of the Particle Identification system is to make a hypothesis about the type of particles that traverse the detector. It consists of two Ring Imaging Cherenkov (RICH) detectors, two calorimeters, and the muon stations that are located at the end of the detector. The most common type of particles identified in the LHCb detector are pions, kaons, and muons. Pions and kaons are the most common hadrons in b decays, therefore it is important to identify them in order to suppress combinatorial background. The identification of muons is also key because they are involved in most of the leptonic and semi-leptonic decays commonly used in LHCb analyses. The advantage of using decays with muons in the final state instead of electrons is their much higher reconstruction efficiency in the energy range relevant for the LHCb experiment.

The RICH detectors

The RICH detectors use the Cherenkov effect to estimate the particles velocity. Together with the momentum measurement of the tracking system, the mass and thus the type of particle can be inferred. They discriminate between pions, kaons, and protons. The Cherenkov effect occurs in a medium with refractive index, n, when charged particles cross it with a velocity, v, larger than the speed of light in the medium ($c' = c/n$). Photons are emitted forming a cone, and the opening angle of this cone ($\cos\theta_c$) is related to the velocity of the particles by

$$\cos\theta_c = \frac{1}{\beta n} \qquad \text{where} \qquad \beta = \frac{v}{c}.$$

Using the momentum value obtained by the tracking system and the mass, the type of charged particle can be determined. In Fig. 3.8 the different opening angles of the cones formed by the different types of charged particles are shown.
In the LHCb detector there are two RICH detectors [17]. The first one, RICH1 is placed just after the VELO that covers the full acceptance of the LHCb, and RICH2 is placed after the SciFi Tracker. RICH1 is designed to cover the full spectrum of particles with momentum up to 50 GeV/c^2, while RICH2 is located further downstream of the detector to cover the particles with higher momentum. RICH1 and RICH2 detectors contain C_4F_{10} and CF_{10}, respectively, as radiator, due to the different range of momentum for which each detector is designed.

The muon stations

The last subdetector are the muon stations. Many of the analyses performed in LHCb involve muons, thus their detection and identification play a key role. The

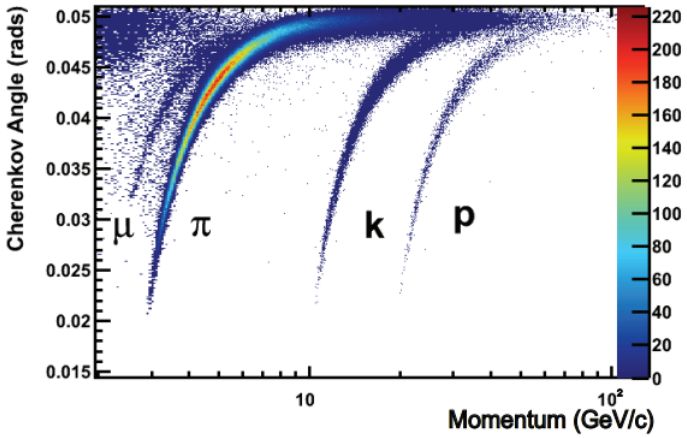

Figure 3.8: Distribution of the opening angles for the different particles that can be identified by the RICH detectors. The plot corresponds to the angles of the cones created by the particles when passing through C_4F_{10}, which is the gas used as radiator in RICH1. Source: [16].

muon system for Run 3 consists of four stations with rectangular shape placed after the calorimeters. Another muon station used to be before the calorimeters in the previous two runs. It was part of the hardware trigger. In Run 3, this station is no longer necessary due to the use of a full software trigger. Removing the first muon station improves however the calorimeter reconstruction due to less scattering between the tracking system and the calorimeter. The muon stations are divided into different regions with different read-out schemes to obtain information about x and y coordinates. The stations contain detection modules, that are made of crossing vertical and horizontal strips.

3.3 The Trigger system

With all the information obtained by the detection systems outlined in the previous section, the whole decay chain up to the pp collision of an event can be reconstructed. However, not all these events are valuable, and not all this information can be stored. In the LHCb, 30 million proton bunches with energies up to 14 TeV collide per second, corresponding to 30 MHz non-empty bunch crossing. This generates a lot more information than the amount that can and needs to be stored. Selecting which events might have some interest and therefore should be saved, is the task of the trigger system. The events which LHCb is interested in are predominantly those containing b or c hadrons.

In the previous runs of the LHC, the LHCb used a three-level trigger. The first one was a hardware trigger called L0 that was able to reduce the rate from 40 MHz to about 1 MHz. It selected events by requiring minimum transverse energy or transverse momentum of the particles. This information was obtained from the

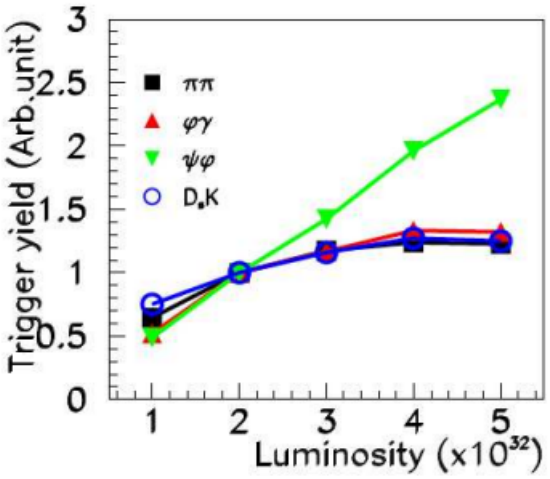

Figure 3.9: The trigger yield for different decays of B mesons. Source: [18].

calorimeters and the muon stations. After this, there was the two-stage software trigger, called High Level Trigger (HLT) which exploited the entire detector to select the interesting events.

In the new trigger strategy for Run 3, the hardware trigger is removed [18]. This decision was made because the cut in E_T that was applied by the L0 trigger, would not be efficient enough to achieve the same output rate for higher luminosities. The threshold would need to be increased and therefore more signal events would be discarded. Fig. 3.9 illustrates how the trigger yield of L0 for a constant output event rate saturates for hadronic final states when the luminosity is increased. Hence, the decision of a full software trigger for Run 3 was made. However, this implies that the detector needs to be readout at 40 MHz and the HLT trigger has to handle a lot higher rates than in the previous runs.
The outline of the trigger system in Run 3 is presented in Fig. 3.10.

3.3.1 High Level Trigger

The HLT [19], as in its previous versions, is divided into two stages. The first stage reduces the rate from 30 MHz to 1 MHz by performing a partial reconstruction of the tracks. The second stage achieves a rate of only few kHz by a full reconstruction and selection of the events. Furthermore, different streams are designed to reduce the size of the events.

HLT1 and track reconstruction

The first stage, the HLT1, aims to reduce the event rate by a factor of 30, from 30 MHz to 1 MHz. After the read out of the detector is completed, the event is passed to HLT1. This first will remove too busy events because they will lead to worse efficiencies. Then, the reconstruction of the tracks starts using the VELO

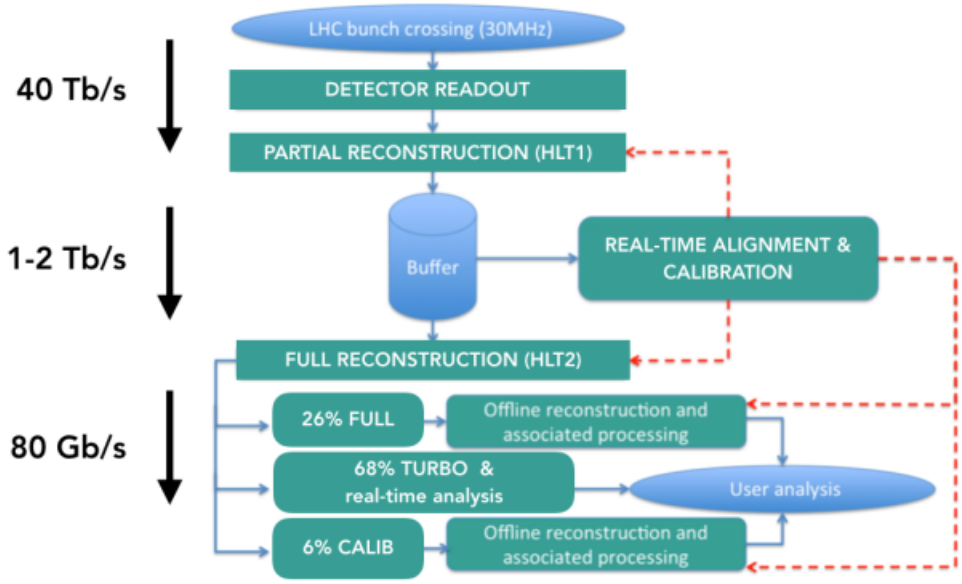

Figure 3.10: Dataflow of the upgrade trigger strategy. The first stage of the trigger reduces the bandwidth up to 1 Tb/s and stores the selected events in the buffer. These are then fully reconstructed in the second stage of the trigger. Finally, part of the selected events are directly stored and other go through the TURBO stream that reduces its size and only keeps relevant information for the analysis. Source: [19].

hits, these are the so-called VELO tracks. In the reconstruction process, there are established different types of tracks. These are classified depending on their interaction with the different subdetectors [20]. Inside the VELO, the magnetic field is negligible, therefore, VELO tracks are reconstructed as straight lines. With these and the position of the beam line, the location of the primary vertices (PV) can be extrapolated. Next, the UT hits are introduced in the reconstruction and the first momentum estimation is obtained. Taking this and the magnetic field model, the tracks are extrapolated to the SciFi, where a better momentum estimation is made. Lastly, a Kalman filter is applied to improve the parameters of the tracks.

Once all these reconstruction steps are ready, several different selections, known as the HLT1 trigger lines, are designed to decide whether the event is worth keeping. The selections depend on the properties of the reconstructed tracks, e.g. the momentum, the goodness of the Kalman fit, the displacement to the PV, etc.

In the whole reconstruction process, apart from the VELO tracks, which are the first ones to be reconstructed, other types of tracks come into play, as more information from different subdetectors is included. These are shown in Fig. 3.11.

The Long tracks are tracks that have traversed the full tracking system, hence they are formed with the combination of hits of all the tracking subdetectors. Since they

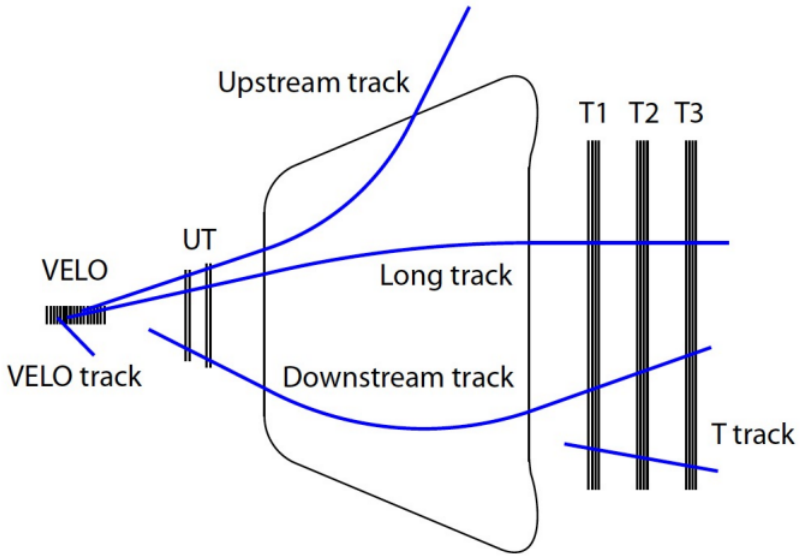

Figure 3.11: Pictorial view of the track types in the LHCb upgrade tracking system. The tracks are classified according to the subdetector whose measurements have been used for the reconstruction. The components of the tracking system shown are the VELO, the UT, the magnet and the SciFi. Source: [20].

are the tracks with the most information, their parameters are best estimated and hence events with long tracks are normally used for analyses.

The Upstream tracks contain information only from the VELO and UT and they correspond to particles that do not arrive to the SciFi Tracker. These are often low momentum tracks, whose trajectory is bent out of the SciFi acceptance.

Finally, the Dowstream tracks are the ones that have interactions with all subdetectors except the VELO. These are normally daughter particles coming from long lived particles that do not decay inside the VELO, such as kaons or Λ particles.

HLT2

The events that passed the HLT1 trigger, are then sent to a buffer. This allows the HLT2 more time to process them. The goal of the HLT2 is to reduce the event rate from 1 MHz to a few kHz.

Before the full reconstruction of the HLT2 starts, real time alignment and calibration are performed. This helps to improve the position and orientation of the detector elements, to ensure better resolution. Thanks to these alignment and calibration processes, the reconstruction carried out at this stage of the trigger is precise enough to be comparable with an offline reconstruction. Therefore, the trigger objects obtained after the HLT2 are already written to disk and can be used for analysis with no need of further offline reconstruction.

In order to achieve the best physics performance with the limited bandwidth of 10 Gb/s, around 70% of the trigger lines used in HLT2 will be exclusive. These are used in the persistency model called TURBO[21] which is designed to reduce the event size. This stream only persists the objects involved in the trigger decision, all the primary vertices, and the additional objects specified in the trigger line. There are different purposes for which it is interesting to save the whole event. For that, around 30% of the events are stored in the FULL stream when at least one trigger selection requires to persist the full event [22].

3.3.2 LHCb software and Monte Carlo Simulations

The study presented in this thesis is preformed using Monte Carlo simulation. These are randomly generated data produced with the goal of behaving exactly as a dataset obtained by the experiment. In order to generate this, two packages of the LHCb software are used, GAUSS [23] and BOOLE. The proton-proton collision is reproduced with the PYTHIA [24] event generator, and GAUSS oversees the physics simulation. The decays of the different particles are generated using the EVTGEN [25] library. Finally, the GEANT4 [26] package is used to simulate the interaction of the particle with the detector. It generates the hits in each subdetector. Afterwards, it is the turn of BOOLE that simulates the subdetectors response to the hits generated in the previous step and converts them into the same output as the readout electronics.

After all these steps, the simulated samples can go through the same process as the data from the experiment. The HLT reconstruction and selection are carried out by MOORE, but the simulated have an extra step in which BRUNEL associates the reconstructed tracks with the generated particle.

4 Motivation and tools for the analysis

This chapter consists of a motivation and an explanation of the analysis tools used for the study carried out in this thesis. In the first section the importance of decay-time dependent analysis for the LHCb physics programme is explained, then the different steps of this type of measurements are outlined. In the final section, the goal of this thesis is discussed.

4.1 Lifetime measurements and decay-time dependent measurements

Lifetime and decay-time dependent measurements form a big part of the analyses performed in flavour physics experiments. The lifetime measurement of hadrons is important to understand the properties of these particles, to test the Standard Model predictions, and to provide inputs to the theoretical calculations. The comparison of measurements with SM predictions is key in the search for physics beyond the SM.

As mentioned before, the LHCb experiment is focused on decays of hadrons containing heavy (b or c) quarks. One of the most predictive tools in quark flavor physics is the heavy quark expansion (HQE) [27]. This technique can predict the decay widths of hadrons containing heavy quarks through an expansion in powers of its inverse mass. Due to the cancellation of several sources of uncertainties, the ratio of the lifetimes is a more precise observable. The comparison of these predictions with the current experimental values is shown in Fig. 4.1. The LHCb has also measured the lifetime of different baryons [28] for example the lifetime of Ω_c^0 [29], which was found to be four times larger than the world average.

Decay-time dependent measurements are also important for similar purposes as the lifetime measurement. One of the most important measurements of this type carried out in the LHCb experiment is the determination of the frequency of the $B_s^0 - \overline{B}_s^0$ system, shown in Fig. 4.2. The parameters of the oscillation systems, are related to the values of the CKM matrix, thus measurements of this type help to estimate the elements of the matrix. CP violation and new physics can contribute to the box diagram of the oscillating systems, thus the comparison of the experimental measurements with the theoretical predictions is important to determine the contributions of these effects.

In summary, the decay-time related measurements are important to move forward in the particle physics paradigm and more precise measurements are expected to

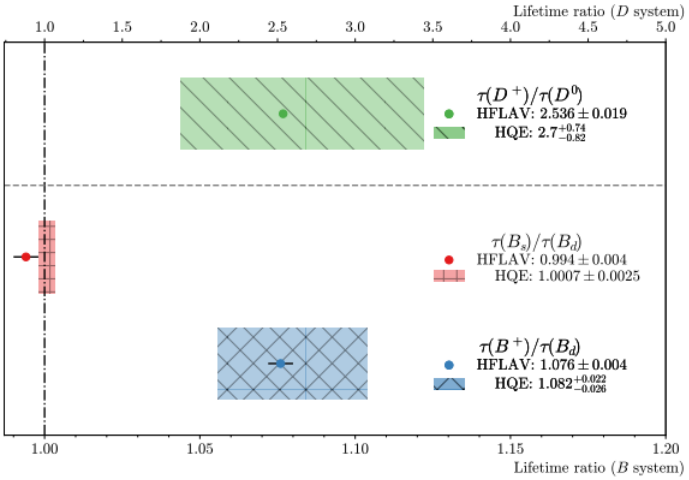

Figure 4.1: Comparison of theoretical predictions (bands), obtained using the HQE model, and the averaged experimental results (dots) for the lifetime ratios, which are the combination of several experimental results. This is shown for different mesons. Source: [30].

be obtained with the data taken during Run 3 of the LHC. The goal of this thesis is to study any alteration that the new detector and new trigger system of the LHCb experiment can have on the decay-time distributions, which might affect the precision of the lifetime and time-dependent measurements.

4.2 Reconstruction of b hadron decay

Before the decay time of a b hadron can be obtained, it is necessary to reconstruct its whole decay. A layout of a b hadron decay to a J/ψ and another hadron can be found in Fig. 4.3. First, all charged stable particles of the decay chain are selected. According to the PID information they are identified as kaons, pions, protons, electrons, or muons. For example, in the decays containing a J/ψ decaying to two muons, all the particles identified as muons will be selected. Then a fit is performed which combines the 4 momentum of the particles to form the intermediate resonances and the B mother particle. After the fit, all necessary information is available, i.e., the masses of the particles, their momentum, their origin and decay vertices, and all the other observables that can be calculated with these.

At this point several cuts are applied to select just the best combinations obtained. These cuts can be for example on the reconstructed mass of the mother particles, a maximum distance between tracks that come from the same vertex, and different quality cuts, for example on the quality of the vertex reconstruction.

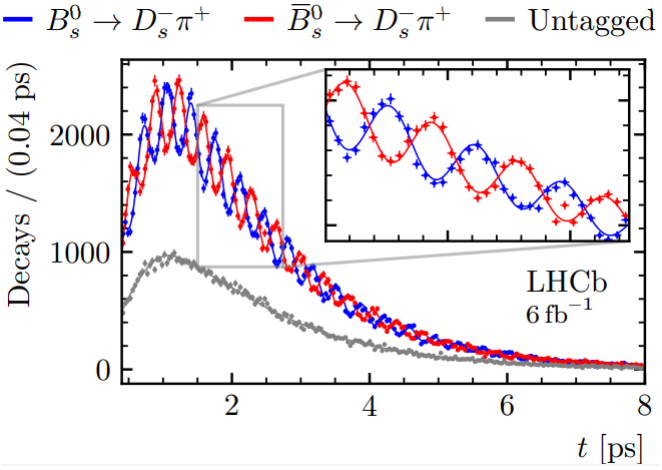

Figure 4.2: Decay-time distribution of the B_s^0 and $\overline{B}_s^0$ mesons decaying to $D_s^- \pi^+$ Source: [31].

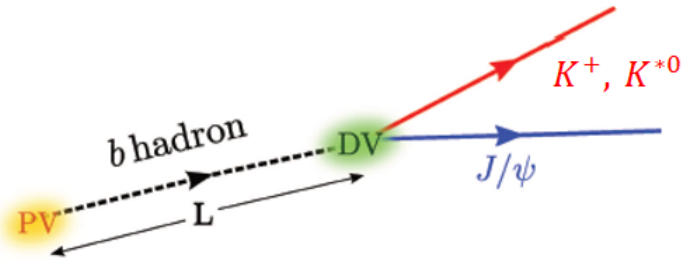

Figure 4.3: Layout of a b hadron decay chain. The hadron is produced at the pp interaction point, PV. It decays into a J/ψ, that decays again to two muons, and into a kaon, that in the case of K^{*0}, decays again into $K^+\pi^-$. The point where the b hadron decays is the secondary vertex, DV. Source: [32].

4.3 Absolute lifetime measurements

Once the b hadron has been reconstructed, using the position of the vertices, the momentum, and the mass, the decay time of each b hadron can be evaluated like

$$t = L\frac{m}{|\vec{p}|}. \tag{4.1}$$

Here L is the distance that the b hadron flies before decaying, $\vec{p}$ is its three-momentum and m is the reconstructed mass of the hadron. Due to the use of the momentum of the b hadron for the decay-time calculation, it is important to reconstruct all the final state particles of the decay to ensure the best estimation of the momentum of the mother particle, the b hadron. This is why fully reconstructed decays are better suited for lifetime measurements, as the one shown in Fig. 4.3. Decays with the presence of neutrinos in the final state that can not be detected, leads to a worse momentum estimation, hence a decay time with larger uncertainty.

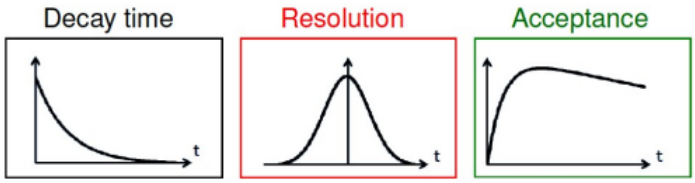

Figure 4.4: Typical shapes of a exponential distribution, a resolution and an acceptance as functions of the decay-time. Source: [32].

The theoretical decay-time distribution follows an exponential distribution. However, when one plots the distribution of the reconstructed decay time, it actually does not correspond to a pure exponential. The exponential is modified due to the effect of the detection and reconstruction processes. First, the obtained distribution includes the resolution. The resolution reproduces the precision of the measured decay times. The origin of the resolution comes from the fact that the magnitudes used for the calculation of the decay time are measured quantities with experimental uncertainties. These uncertainties are due to several factors: first, the resolution of the detector, which depends for example on the designed granularity of the detector or on the performance of the electronics; and second, the uncertainty of reconstruction of the tracks, in which the different magnitudes are evaluated, that can be affected by scattering or material effects.

Furthermore, the reconstruction and the selection can modify the decay time distribution. This occurs when candidates that correspond to a certain region of the decay time distribution, are less likely to be selected than candidates with other decay times. The possible causes are the geometry acceptance of the detector, the pattern search in the track reconstruction, or the cuts applied. For example, a cut on the displacement of the b hadron vertex from the beam line is more likely to cut away candidates with a short decay-time, and this then changes the distribution. This effect is described by the decay-time acceptance, which is the probability for a candidate to be selected as a function of its decay time.

All things considered, the distribution obtained for the measured decay time is composed of three ingredients: the pure exponential distribution, the resolution $\mathcal{R}\,(t)$ and the acceptance Acc (t), combined as follows:

$$f(t) = \left[\mathrm{e}^{-(t/\tau)} \otimes \mathcal{R}\,(t)\right] \times \mathrm{Acc}\,(t), \tag{4.2}$$

where the exponential is convoluted with the resolution and then is multiplied by the acceptance. The typical shapes of an exponential distribution, the resolution and the acceptance can be found in Fig. 4.4. For the acceptance, just the shape is important, since a constant value can be included in the normalization factor of the final distribution.

Finally, with well-described acceptance and resolution, the lifetime of B meson can be obtained by performing a fit to the measured decay-time distribution according to Equation 4.2.

4.4 Maximum likelihood fit

The fit to the decay-time distribution is performed in this analysis using the maximum likelihood method. There is the data sample with n points, which in this case they would be the different b-hadron candidates considered for the fit. Each of these points has an array of observables $\vec{x}$, which in this case is just the decay time t, the only magnitude used in the fit. The distribution of these observables is given by their probability density function (PDF), $\mathcal{P}(\vec{x}|\vec{\theta})$, where $\vec{\theta}$ is the array of parameters that the PDF has. In the case of this analysis, when fitting the decay time distribution, the only parameter is the lifetime τ. Therefore, the likelihood function $\mathcal{L}(\vec{\theta})$ is defined as the product of the PDFs of all reconstructed candidates

$$\mathcal{L}(\vec{\theta}) = \mathcal{L}(\tau) = \prod_{\mathrm{i}}^{n} \mathcal{P}(x_{\mathrm{i}}|\tau),$$

where, in this case x_{i} are the different values of decay time. The likelihood corresponds to the probability to obtain the measured distribution of decay times for a certain value of τ. Hence, to obtain the most likely value of τ of the measured distribution, one just needs to maximize the likelihood. Due to computational reasons, the negative logarithm of the likelihood is minimized instead

$$-\ln \mathcal{L}(\tau) = -\sum_{\mathrm{i}}^{n} \ln \mathcal{P}(t|\tau).$$

In this analysis this minimization is performed using the MINUIT framework [33].

4.5 Lifetime bias in Run 1

In the previous sections the relevance of the lifetime measurements and how they are obtained, have been described. As it has been explained in Section 4.3, in order to perform a correct fit to measure the lifetime, it is necessary to, first, obtain the acceptance of the whole process, i.e., the reconstruction, the selection and the trigger. All the time-related analyses mentioned in Section 4.1 were carried out with data obtained in the previous runs of the LHC. To get valuable results, these analyses needed an accurate estimation of the acceptance. One of the first analyses in which the decay-time acceptance was analysed in detail was the measurement of the lifetime of several b hadrons [32]. It was found that the acceptances of the selection of several b hadrons were highly dependent on the decay-time, as it can be

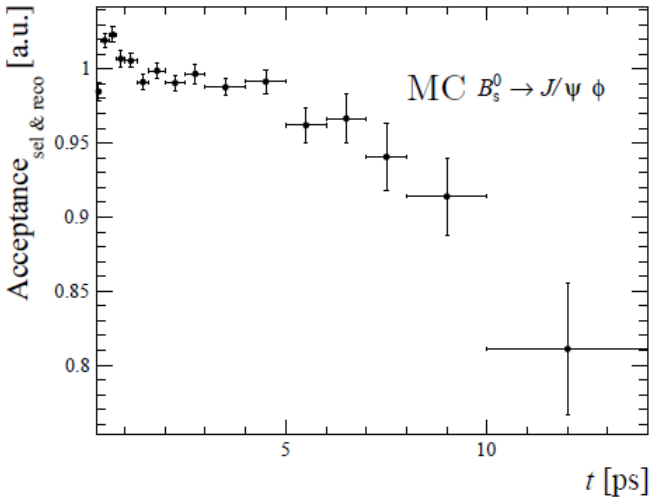

Figure 4.5: Acceptance obtained after the reconstruction and selection of the $B_s^0 \to J/\psi\ \phi$ candidates. Source: [32].

seen in Fig. 4.5 for the $B_s^0 \to J/\psi\ \phi$ channel. Similar effects were also observed for other channels such as $B^+ \to J/\psi\ K^+$ or $B^0 \to J/\psi\ K^{0*}$.

To understand the source of this problem and to be able to correct it, the effect was studied in detail in simulated samples. All the steps of the process that real data undergoes from its detection to its analysis were mimicked one by one in simulated samples. Any effect that each of these steps had in the shape of the decay-time distribution and therefore, in the acceptance, was measured. Finally, a global bias of almost -20 fs was found in the three studied channels. The main source of this bias was found to be in the reconstruction of the VELO tracks. Due to the geometry of the sensors used in the previous version of the VELO, outlined in Section 3.2.1, and the only approximately correct assumption of the reconstruction algorithm that most of the b hadrons are created close to the beam line, the tracks displaced far from the beam line were not properly reconstructed. These displaced tracks correspond to hadrons that have traveled a longer distance before decaying and hence have a longer decay time. Therefore the VELO reconstruction had a lower efficiency at higher decay times.

4.6 Importance of the current lifetime bias study

The goal of the present thesis is to perform the same study of the lifetime bias, as the one mentioned in the previous section. Instead of being part of a measurement, as it was in Run 1, the study of lifetime bias is carried out at an earlier stage of Run 3. It is vital to ensure unbiased reconstruction and least-biased selections before the real data taking for Run 3 as the new event model only persists partial information of

the selected event, in which case it is impossible to correct the bias of reconstruction offline.

This study is necessary as significant upgrades of the detectors and changes of reconstruction algorithms are carried out for Run 3, as described in chapter 2. Among these changes, one of the biggest differences from Runs 1 and 2 is the mentioned elimination of the hardware trigger, which will force the software trigger to handle much higher amounts of data. This implies the need of a better pattern recognition strategy in the VELO to achieve a similar performance as the old version but at much higher rates. Therefore, the new VELO consists on pixel sensors, instead of the old strip sensors, and accordingly new pattern recognition algorithms have been designed. Another feature that can change the performance of the detector is the increase of the pile-up, i.e. a higher density of particles inside the detector. To encounter these changes, new software techniques and algorithms are implemented to optimize the reconstruction, the selection and, the trigger, which might cause some bias in the measurement of lifetime.

5 Analysis strategy

This chapter contains a detailed description of the decay-time bias study. In the first section the simulated data samples used are explained. Later the results obtained about the effects of the reconstruction in the decay-time distribution are presented. Finally, the performance of the decay-time reconstruction is evaluated.

5.1 Decay modes and data samples

In order to study any time-dependent bias that can be introduced in the processing of the data, the different steps of the reconstruction, selection, and trigger are applied to MC samples and the effects that these have on the decay time distribution are analysed. MC datasets are useful for this kind of study since they are performed as preparation for Run 3 of LHC before the data acquisition starts. Furthermore, the key feature of the MC samples is that the input is known, hence the real values of the observables can be compared with the ones obtained in the data processing. This is thanks to the fact MC datasets are produced such that they can undergo the same processes as real data, i.e. they can have reconstructed observables obtained with the same algorithms as real data, and trigger selections can also be applied to them. One example of this which is key for this study are the values of b-meson decay-times. The decay-time values contained in the MC sample are called true decay times and are represented by t_{MC}. For each B meson in the MC sample one can access the value of the true decay time. The reconstructed decay times t_{rec} are only obtained after the reconstruction algorithms are executed. These are the only decay time values available when a lifetime measurement is performed with real data.

For this study, the same channels that were used in previous analyses for the measurement of b-mesons lifetime are used [32]. These are $B^+ \to J/\psi\ K^+$ and $B^0 \to J/\psi\ K^{*0}(\to K^+\ \pi^-)$, where $J/\psi \to \mu^+\mu^-$. There are several reasons for the choice of these channels for the b-meson lifetime measurement. Both decay modes have stable particles in the final state that can be detected. They also contain a J/ψ, that decays almost instantaneously to two muons with a branching ratio[1] of $\mathcal{BR}\ (J/\psi \to \mu^+\mu^-) = (5.961 \pm 0.033) \times 10^{-2}$. Although the hadronic decays of the J/ψ have a higher branching ratio, the decay to two muons is cleaner and therefore easier to select. Decays to electrons are not used because their reconstruction efficiency and momentum resolution are a lot worse due to bremsstrahlung and lower resolution in the calorimeters. In addition, using channels with a J/ψ decaying to

[1] All values of the branching ratios are obtained from [34]

two muons allows to benefit from the good performance of the muon system of the LHCb detector, which has a high reconstruction efficiency.

The study is performed first with the $B^+ \to J/\psi\ K^+$, because it has three final state particles, one less than the B^0 channel, and therefore is easier to reconstruct. This decay has a branching ratio of $\mathcal{BR}\ (B^+ \to J/\psi\ K^+) = (1.020 \pm 0.019) \times 10^{-3}$. The study continues with the decay $B^0 \to J/\psi\ K^{*0}$, where the excited state of the K^0, K^{*0}, decays almost instantaneously to a kaon and an oppositely charged pion, $K^{*0} \to K^+\pi^-$. The total branching ratio of the B^0 decay channel is $\mathcal{BR}\ (B^0 \to J/\psi\ K^{*0}) = (1.017 \pm 0.05) \times 10^{-3}$. For both decay channels, the MC samples used contain around three million events.

5.2 Search for lifetime biases

The goal of the study is to prove whether any cut applied or any algorithm used in the processing of the data introduces a decay time bias. For that, the same technique as the one used in Run 1 [32] is used. The different steps of the processing of the data are applied to simulated samples one by one. In order to check if the shape of the decay time distribution is affected by any of the steps, a fit is performed to obtain the lifetime. A change of the lifetime obtained after one step has been applied would mean that it introduces a bias.

The process from the proton-proton collision inside the VELO detector till the data is ready for its analysis can be divided into three stages: the reconstruction, the selection, and the trigger. The reconstruction is the process in which the tracks and other magnitudes of the stable particles like the momentum or the mass are calculated using the information from the different subdetectors. This stage contains the first five steps of the study, in each of them several cuts are applied. The possible origin of a time bias at this stage are geometrical issues in the track reconstruction, e.g. problems in the pattern recognition (i.e. how hits are searched and combined), the geometrical acceptance of the detector, or bad performances of the electronics in certain regions of the detector.

Next, the reconstructed stable particles are combined to reconstruct the rest of the decay chain, i.e. the intermediate resonances, the b meson, the vertices, etc. This process is called selection. The possible sources of lifetime biases at this stage are multiple due to all the different algorithms used to obtain the different observables. One potential cause is the PV reconstruction because its position is involved in the flight distance calculation which is used in the decay time measurement as shown in Equation. 4.1.

Finally, in the last two steps of the study, a collection of cuts applied together in the trigger lines is checked.

The study is first performed analysing the distribution of true decay times present in the MC sample. The goal of this is to analyse first whether any step of the data

processing has an efficiency dependent on the decay time of the b hadron. After this has been evaluated, the effect of each step on the calculation of the decay time is studied. The latter study is presented in Section 5.3.

5.2.1 Decay-time acceptance

In the cases in which after applying a set of requirements, the obtained lifetime changes in comparison with the previous step, the changes in the decay-time distribution need to be studied. This is done using the acceptance plot[2], which is obtained by dividing the decay-time distribution of the B candidates before and after applying the cuts under study. This can be better understood with Fig. 5.1, which illustrates the acceptance of a set of cuts on the transverse momenta of the final state particles of the $B^+ \to J/\psi\ K^+$ channel (step 1). In Fig. 5.1 (a), the blue dots represent the true decay-time distribution of all candidates contained in the simulated sample, and the orange ones correspond to the remaining candidates after the cuts are applied. To obtain the acceptance represented in Fig. 5.1 (b), these two distributions are divided. Before dividing the distributions, they are re-binned such that all of the bins have a comparable amount of B candidates and hence a similar uncertainty. More precisely, the bins used for Fig. 5.1 (b) are defined with logarithmic scale in base equal to 1.638, which in picoseconds is the global average for the lifetime of B^+. Therefore a perfect exponential distribution $f(t) = 1/\tau \exp(1/\tau)$ with $\tau = 1.683$ ps would have the same number of events in each bin. The meaning of the acceptance plot lies in its shape, and not in its absolute values. In Fig. 5.1 (b), it can be observed that it is effectively flat, thus this serves as visual proof that no important bias is introduced in the first step of the reconstruction.

5.2.2 True decay time study

The first fit is performed in step 0, where all the events of the simulated sample are present in the decay-time distribution because no requirement has been applied yet. The decay-time distribution obtained at this step for the $B^+ \to J/\psi\ K^+$ channel is shown in Fig. 5.2. In this figure the fit performed to obtain the lifetime is represented in blue. The fitted function is just a normalized exponential $f(t) = 1/\tau \exp(-t/\tau)$. This is done using the Likelihood method explained in Section 4.4. The lifetime obtained in the fit is $\tau = (1.6395 \pm 0.0009)$ ps, which corresponds to the first point in Fig 5.3a, in which the dashed lines of the plot corresponds to the global averaged value used in the MC generation of the meson lifetime $\tau(B^+) = (1.638 \pm 0.004)$ ps [35]. The equivalent result is shown for the B^0 channel where the global average value is $\tau(B^0) = (1.519 \pm 0.004)$ ps. The agreement between the result of the fit and the established values serves as validation of the fit procedure.

[2]For the rest of this thesis, the word acceptance will refer to decay-time acceptance. Other types of acceptance are clearly specified.

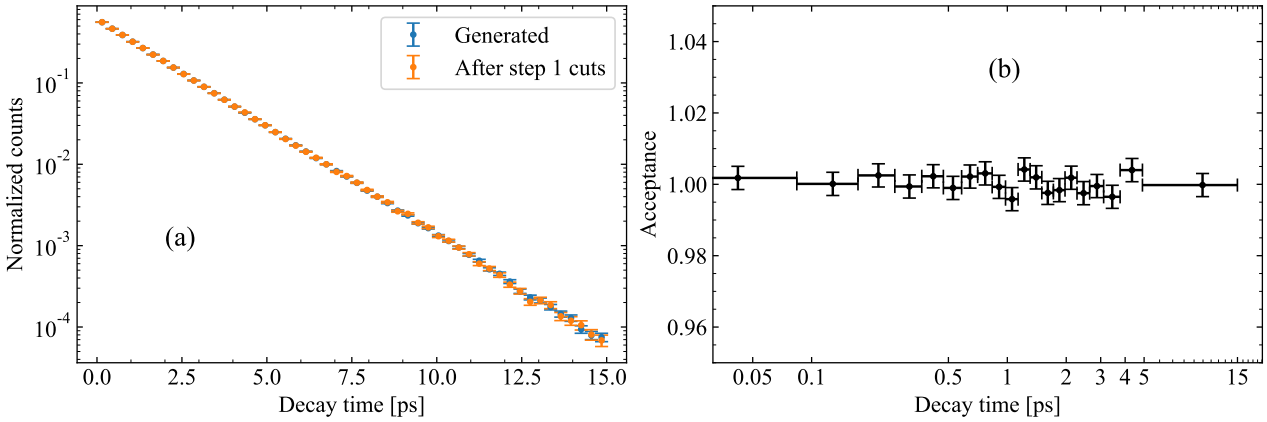

Figure 5.1: (a) Decay-time distribution of all the events present in the $B^+ \to J/\psi\ K^+$ MC sample (blue) and the events that pass the requirements of the first step of the reconstruction (orange). (b) The ratio of both distributions present in (a).

The values of the lifetime obtained after applying each of the steps are presented in Fig. 5.3. The data points of each plot are highly correlated because the candidates after one step is applied are also present in the previous step, i.e, the study starts with a complete sample in step 0 and candidates are removed from it step by step according to the different requirements. Each result is analysed individually later in this section but first, some preliminary observations can be extracted from these plots. First, it can be observed, that no relevant overall bias is introduced, since the value of the lifetime obtained in the last step when all the requirements have been applied is very close to the initial value. In both cases, the difference of the lifetime in the first and last step is around 1 fs, which taking into account the statistical uncertainties, is negligible. Also, it is not significant compared to the bias of around 20 fs found in the previous version of this study with the Run 1 data.

Another positive result that can be extracted from these figures is that the small changes in the lifetimes, that are analysed later, are the same for both channels. This is an important observation because it means that the fact that one channel has one more particle in the final state, and therefore a more complicated reconstruction, does not modify the decay-time distribution. The only difference that this implies is that when the selection takes place, and the mother particles are reconstructed, there is a lower total efficiency in the case of the $B^0 \to J/\psi\ K^{*0}$, and therefore worst statistics after step 6, as can be observed in Fig. 5.3b.

Step by step study

In the following, the effect of each step is analysed. In Appendix A there is a complete list with the requirements of each step. The cuts applied to the samples

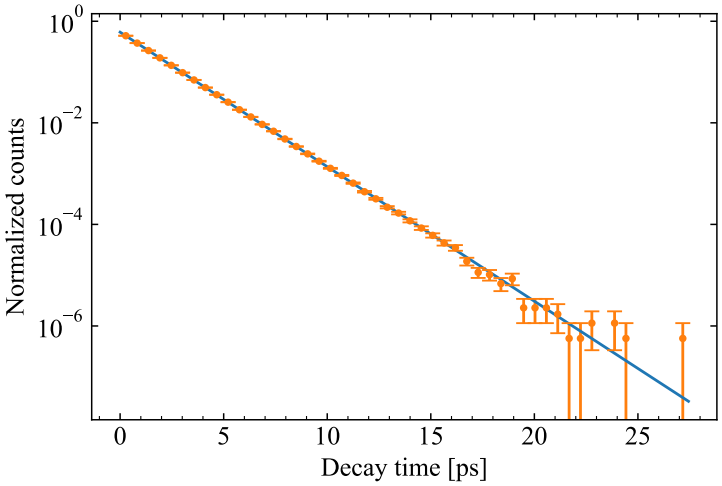

Figure 5.2: The distribution of the decay-time values of all the b mesons present in the MC sample is displayed in orange. The blue line represents the result of the lifetime fit.

in step 1 are minimum cuts on the transverse momenta of the final state particles. Again, since the reconstructions algorithms are not yet executed at this stage, these cuts are applied on observables from the simulation. The goal of these requirements is to simulate the fact that tracks with too low momentum are more likely to be outside of the detector acceptance because their trajectory is bent, and therefore are not reconstructed. Furthermore, in the low momentum region there is large background coming from the beam, hence the cuts are essential for any analysis. These requirements do not introduce any bias.

The next two steps, 2 and 3, are about the reconstructibility of the tracks. This is a variable that can be obtained from the simulated samples. It states as which type of track each final state particle can be reconstructed, which depends on the number of hits each particle leaves in the different subdetectors. For instance, for a particle to be reconstructed as a VELO track it is required at least three hits in the VELO [36]. The different types of tracks and their relations with each tracking subdetector is pictured in Fig. 3.11.

In both cases, in Fig. 5.3a and Fig. 5.3b, it can be observed how a small bias of around 2 fs is introduced in step 2 when all the final state tracks are required to be reconstructible as VELO tracks. The particles that do not have enough hits in the VELO are mainly produced by b mesons that have a long decay time and hence they decay outside of the VELO preventing the stable particle from leaving hits in the VELO. Therefore by cutting away B candidates whose final state particles cannot be reconstructed as VELO tracks, mainly long-decay time candidates are removed, and a bias is created. This can be seen in Fig. 5.4, where the acceptance of the requirement of step 2 with respect to step 1 is clearly lower for decay times higher than 4 ps.

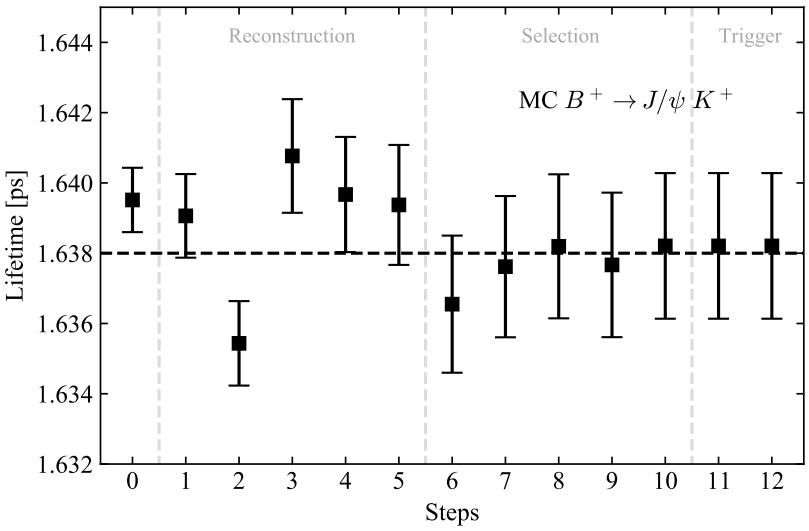

(a)

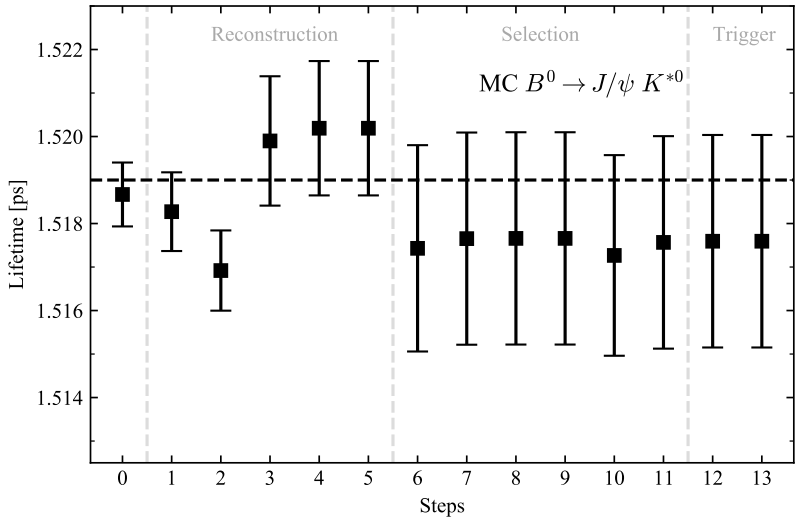

(b)

Figure 5.3: Measured lifetime in simulated Monte Carlo samples of $B^+ \to J/\psi\ K^+$ and $B^0 \to J/\psi\ K^{*0}$ after the different requirements of the reconstruction, the selection and the trigger are applied sequentially. The steps are individually explained later in this section. The dashed lines correspond to the average values of the lifetimes of each meson.

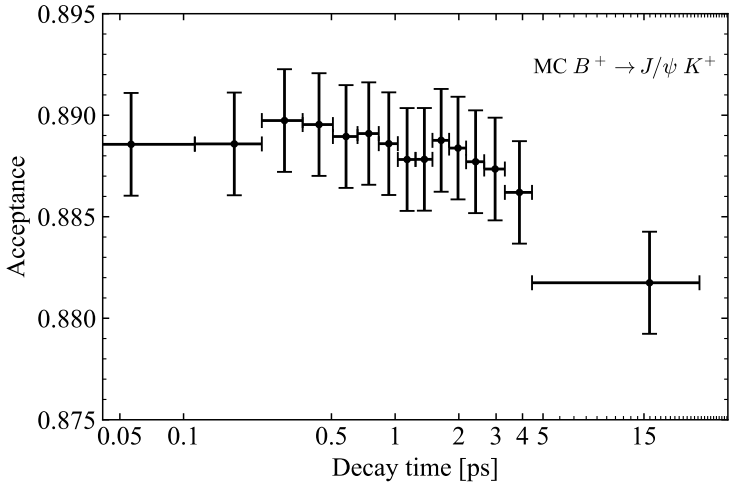

Figure 5.4: Acceptance of the step 2 with respect to the step 1.

In step 3, an opposite bias is introduced which corrects the previous one. This implies that in step 3 the value of the lifetime is in agreement with the one obtained in step 0. The requirement of step 3 is that all the final state particles are reconstructible as long tracks. For that, it is required that a particle is reconstructible as a VELO track and that it has left a minimum number of hits in the SciFi Tracker. This requirement removes mainly events with shorter decay times, which is suggested by the acceptance of this step with respect to the previous one, shown in Fig. 5.5. Final state particles produced at large opening angles are more likely to be outside the SciFi acceptance if their production vertex is located at smaller z values. These correspond more likely to daughter particles of short-lived B mesons.

Since the origin of these biases is due to the geometry of the decay chain, they can be avoided if only events whose particles have pseudorapidity (η) within a certain range are used. This is something that is normally required in all the analyses of the LHCb experiment. The events that are in the tails of the pseudorapidity distribution have a lower reconstruction efficiency, especially when they have very long or very short decay times. This is clearly visible when looking at the pseudorapidity acceptance of the muons of step 2 with respect to step 1 shown in Fig 5.6 right, which demonstrates that events cut away by the requirement of VELO track reconstructubility are mainly in the tails of the pseudorapidity distribution. The requirement of step 2 would not have such an effect if before the analysis a fiducial region is defined as $2 < \eta < 4.5$.

In steps 4 and 5 the requirements are that all the final state particles are reconstructed as VELO and as long tracks, respectively. This is not introducing any significant bias as can be seen in Fig 5.3. In steps 2 and 3, just a minimum number of hits in the subdetectors was required. For steps 4 and 5 it is required that the algorithms reconstruct successfully all the final state particles as these types of tracks. Step 4 was the main source of bias in Run 1. The problem came from a not

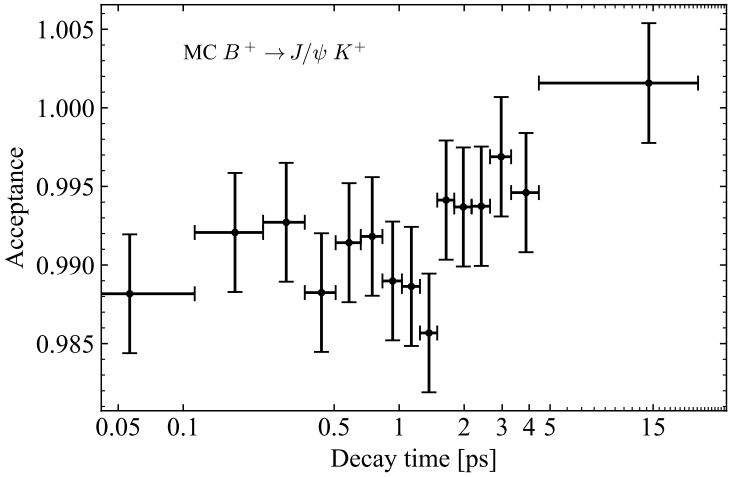

Figure 5.5: Acceptance of the step 3 with respect to the step 2.

completely correct geometrical assumption in the reconstruction algorithm of the VELO tracks. It was assumed that the tracks of the final state particles have their origin around the interaction region. This is not the case for the events in which the b meson flies a long distance before decaying. Therefore the final state particles of the events with long-lived b meson were not properly reconstructed as VELO tracks, and these events were cut away in step 4. This introduced a bias of around 14 fs in the Run 1 analysis.

In the next steps the requirements are about the reconstruction of intermediate particles, i.e, J/ψ and K^{0*}, and the B meson. To obtain these, the different tracks of the final state particles are combined. This process is carried out by the Moore application, mentioned in Section 3.3.2. The goal of this application is to carry out the reconstruction and select the signal events by applying the trigger lines. Moore is used as part of the online data processing in Run 3 [37]. In the rest of this section, the effect that the efficiency of reconstruction can have on the true decay time distribution is studied. Therefore, after the reconstruction, only candidates that are linked to a simulated B meson are used. In Section 5.3, the performance of the reconstruction of the decay times of each b hadron is evaluated.

First, just the effect of the reconstruction of the whole decay chain is checked, i.e. no further cuts are applied. For that the simulated sample is processed with Moore using trigger lines with very loose requirements, so the only possible effects on the decay-time distribution are due to the loss of B candidates that fail the reconstruction. From the output of running Moore with the loose trigger lines, only the candidates that are present in step 5 are selected. This implies fake combinations are excluded. For both decay modes a bias of around 3 fs is visible in this step (step 6, Fig. 5.3). In Fig. 5.7 the acceptance between step 5 and step 6 is shown. The

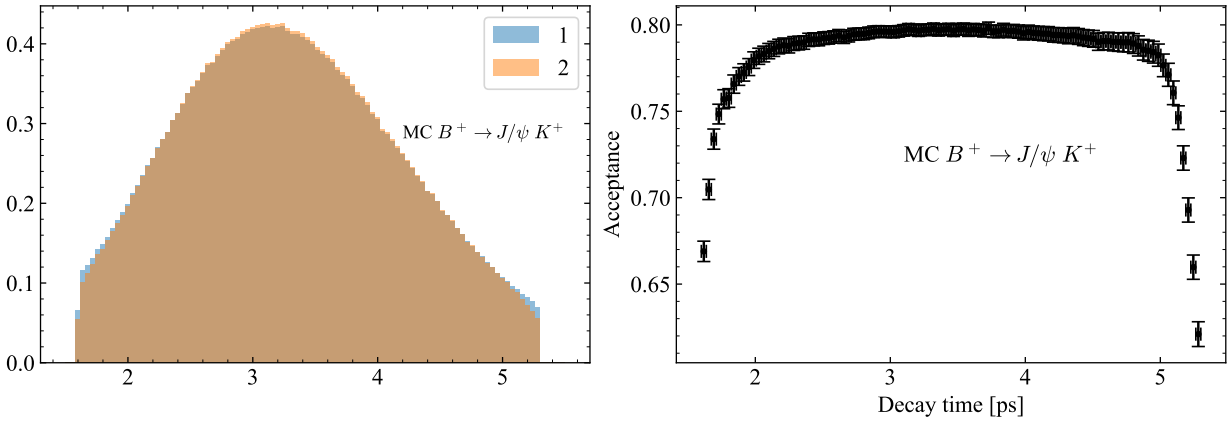

Figure 5.6: (left) Histograms of the pseudorapidity of the muons of the events present in step 1 and in step 2. (right) Acceptance of the requirement of step 2 as function of the pseudorapidity. It is obtained by dividing the two distributions of the right plot.

shape of these plots does not suggest that the efficiency of the reconstruction carried out by MOORE has a strong dependence on the true decay time of the b meson.

The origin of this small bias can be multiple factors because multiple algorithms process the sample when MOORE is executed. Concerning the multiply possible causes and because the bias introduced is small compared to the statistical uncertainty of the result of the fits, which even they are correlated, increases in step 6 due to a loss of statistics, no further analysis of this bias is done.

The next steps of the selection before the Trigger stage contain requirements used to select the signal candidates. These include cuts in the quality of the vertices, the reconstructed mass, and the momentum of the intermediate resonances and b mesons. There are also requirements for the identification of the type of the final state particles. These steps do not introduce any bias.

The last two steps correspond to the requirements of two trigger lines shown in Table 5.1. These lines were used in the Run 1 and Run 2 measurements of the b meson lifetimes for the selection of the J/ψ candidates. These trigger lines do not introduce any decay-time bias.

The simulated samples used for the study are produced using two opposite polarizations of the magnet. There exits the sample with the up and down polarizations, corresponding to the positive and negative direction of the y axis, respectively. In the results shown in Fig. 5.3, the two samples are combined. The same study is also performed for each polarization separately to check if any of the requirements has a different effect depending on the polarization of the magnet. The results obtained are shown in Fig. 5.8. In these plots, no significant differences in the behaviour of the two polarizations are observed. In Fig. 5.8b, in step 11 the obtained lifetime

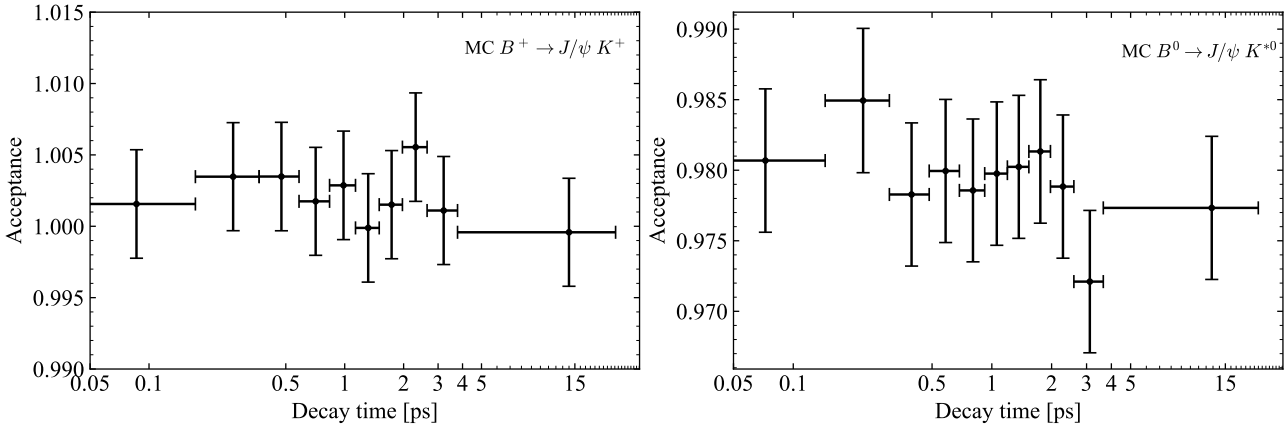

Figure 5.7: Acceptance after reconstructing the whole decay chain using MOORE (step 6 with respect to step 5.

Table 5.1: Selections of the HLT1 and HLT2 lines useful for the selection of the J/ψ candidates.

	`HLT1DiMuonHighMass`	`HLT2DiMuonJPsi`
p_T [GeV/c]	$>$ 0.5	-
p [GeV/c]	$>$ 6	-
χ^2_{track}/nDoF	$<$ 4	$<$ 5
DOCA [mm]	$<$ 0.2	-
$m(\mu^+\mu^-)$[GeV/c^2]	$>$ 2.7	$\text{M}_{J/\psi} \pm 0.12$
χ^2_{vtx}/nDoF	$<$ 25	$<$ 25

for B^0 increases with respect to the previous step for the up polarization, while decreases for the down. This behaviour is not observed in the corresponding step of the B^+ channel (step 10), thus this can be simply considered as an effect of the large uncertainties at that point of the study.

In this section, all the possible sources of lifetime bias have been studied. Only bias of at most 3 fs has been found, which is a really positive result in comparison with what was found in the same study in Run 1, where biases of the order of 15 fs were found. The most important bias is found when the reconstructiblity of the final state particles is required. This can be corrected if only particles with a value of pseudorapidity within a certain range are used for the analysis. To show this, the study has been repeated by including in step 1 the requirement that the final state particles have pseudorapidity larger than 2 and lower than 4.5. The results obtained when this extra requirement is applied are presented in Fig. 5.9. Here, the requirements of reconstructibility of step 2 and step 3 are not a source of bias anymore. The reason for this is the low reconstruction efficiency of the particles outside this psuedorapidity interval.

5.3 Reconstructed decay time

In the previous section, the goal was to check whether the acceptance of the requirements of the reconstruction, the selection, and the trigger have a dependence on the decay time of the b hadron. For that, the true decay-time values from the simulated samples were studied. Now, the study focuses on the reconstructed decay times which are calculated according to Equation 4.1 relying on the measured position of the vertices and the momentum of the particles. This section aims to prove if the requirements have an effect in the evaluation of the decay time and on its distribution, which is fitted to obtain the lifetime.

The function that should describe the distribution of reconstructed decay times in the case of a flat acceptance is a convolution of a pure exponential and the resolution. This is the expression between brackets shown in Equation 4.2. The resolution is the function that describes the precision of the decay time measurement. The convolution of the pure exponential and the resolution is the function that is used to fit the reconstructed decay times distribution to obtain the lifetime in each step.

The function that describes the resolution is obtained by a fit to the distribution of the differences between the true decay time, t_{MC}, and the reconstructed decay time, t_{rec}, of each B candidate. In this study, the resolution is evaluated after the requirements of each step have been applied. It is first obtained in step 6 after the reconstruction application MOORE is executed. This is shown in Fig. 5.10 for the B^+ channel, where for the fit, the sum of three Gaussian distributions with common

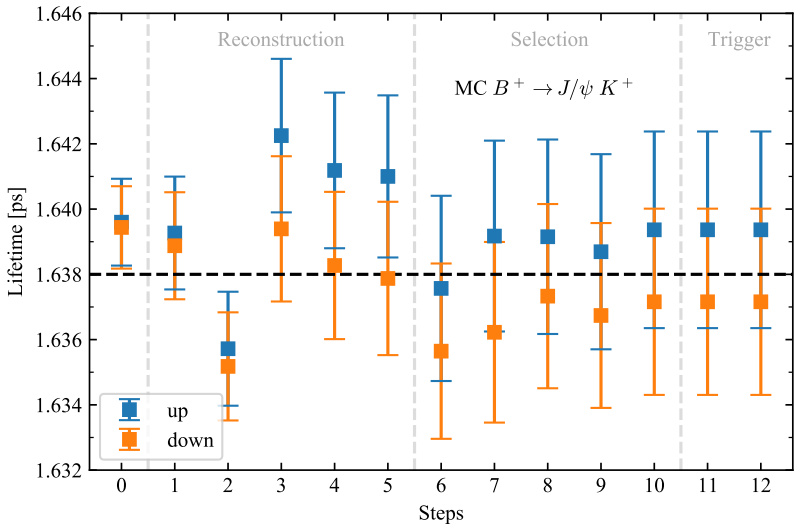

(a)

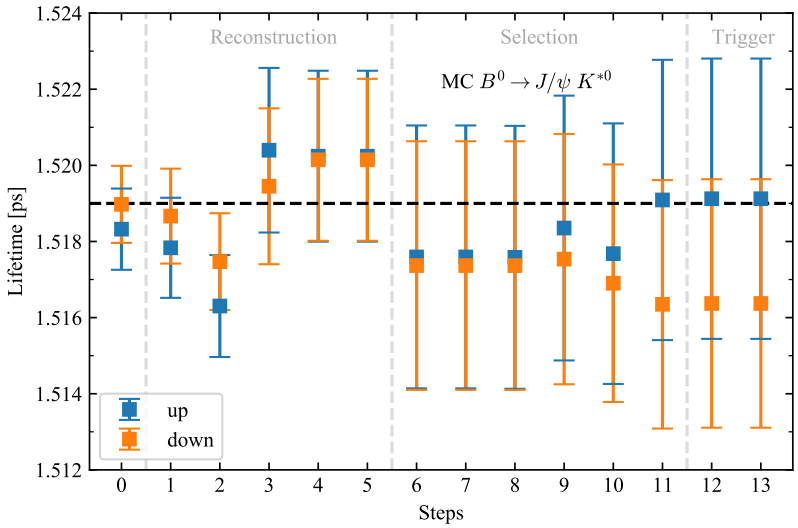

(b)

Figure 5.8: Results of the study of lifetime bias for the each polarizations of the channels $B^+ \to J/\psi\ K^+$ and $B^0 \to J/\psi\ K^{*0}$. The dashed lines correspond to the global average values of the lifetimes of each meson.

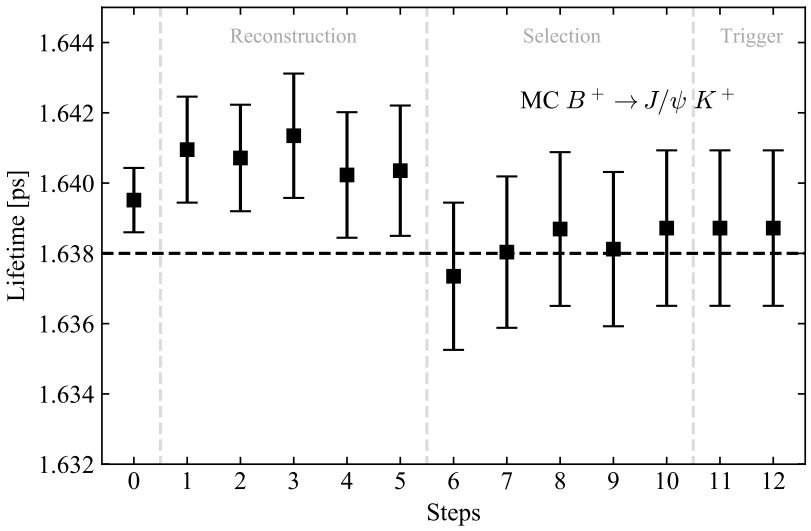

(a)

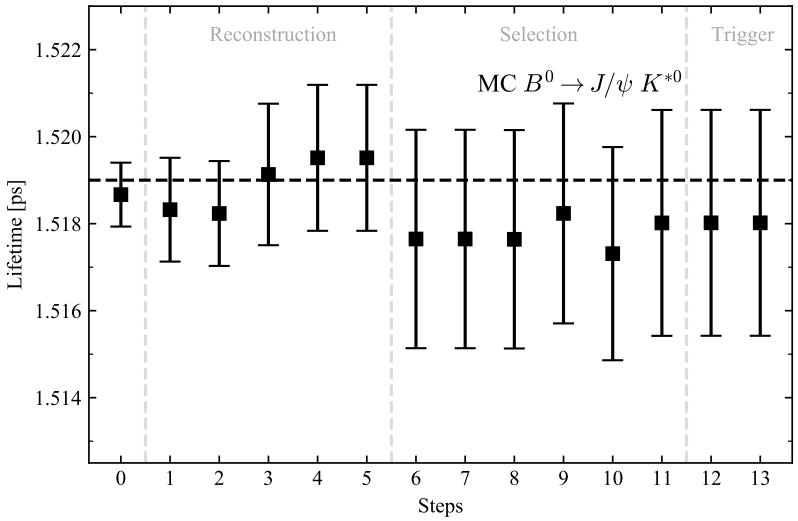

(b)

Figure 5.9: Results of the study of lifetime bias when in step 1 an extra requirement of $2 < \eta < 4.5$ is applied for all final state particles.

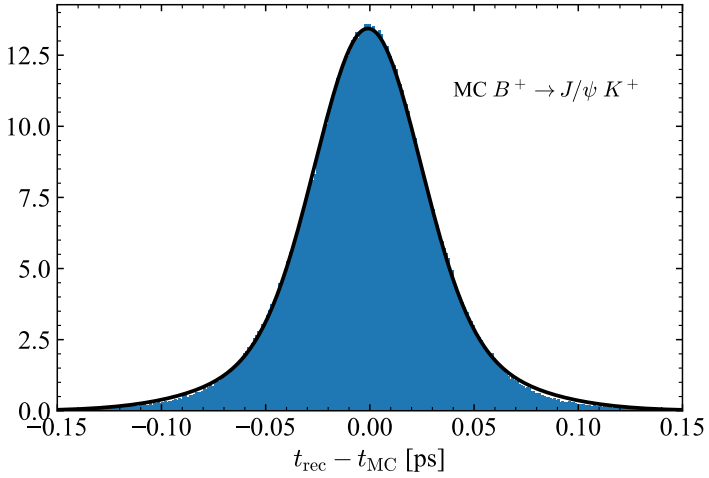

Figure 5.10: In blue, the histogram of the differences between the simulated decay time and the reconstructed one. In black, the sum of three Gaussian distributions with common mean value fitted to the distribution.

mean value is used. To obtain a better description of most B candidates, a range of (-0.2, 0.2) ps of the decay time difference $t_{\rm MC}$-$t_{\rm rec}$, is selected for the fit.

The mean value obtained in the fit is (-0.939 ± 0.04) fs. This value is small compared to biases of few femtoseconds which are present in the study. The fact that the mean value of the Gaussian distributions is close to zero is important because it implies that the reconstruction is not shifting the reconstructed decay time values to higher or lower decay times.

The same procedure is repeated after the requirements of each step are applied. The parameters of the three Gaussian distributions that fit the resolution are shown in Tables 5.2 and 5.3 for the B^+ and the B^0 channels respectively. In the case of the B^0 channel, although the reconstruction application MOORE is executed in step 6, is not until step 10 that the reconstruction of the b meson is required. In these tables, it can be observed that the requirements of the last steps do not introduce relevant modifications in the resolution. This is an important result because a change in the mean value of the resolution would indicate a bias in the reconstruction of the decay time.

Another observation is that the small shift of the mean value from zero remains in every step. Therefore, this is not a statistical fluctuation and implies that the reconstructed decay times values are slightly smaller than the values from the simulated sample. This issue is not relevant for two reasons; first because is a really small shift, and second, because the fact that the convolution of the exponential distribution and the resolution is used to obtain the lifetime, corrects this shift.

Table 5.2: Parameters obtained in the fit of the resolution for the B^+ channel.

Step	μ [fs]	f_1	σ_1 [fs]	f_2
6	-0.94 ± 0.04	0.286 ± 0.018	20.6 ± 0.3	0.087 ± 0.002
7	-0.90 ± 0.04	0.297 ± 0.019	20.7 ± 0.3	0.081 ± 0.003
8	-0.92 ± 0.04	0.291 ± 0.019	20.8 ± 0.4	0.082 ± 0.003
9	-0.93 ± 0.04	0.32 ± 0.02	21.2 ± 0.3	0.076 ± 0.003
10	-0.93 ± 0.04	0.34 ± 0.02	21.4 ± 0.3	0.066 ± 0.003
11	-0.93 ± 0.04	0.34 ± 0.02	21.4 ± 0.3	0.066 ± 0.003
12	-0.93 ± 0.04	0.341 ± 0.018	21.4 ± 0.3	0.066 ± 0.003

Step	σ_2 [fs]	$1 - f_1 - f_2$	σ_3 [fs]
6	70.4 ± 0.5	0.627 ± 0.018	33.2 ± 0.3
7	69.5 ± 0.6	0.622 ± 0.019	33.3 ± 0.3
8	69.6 ± 0.6	0.626 ± 0.019	33.4 ± 0.3
9	67.1 ± 0.6	0.60 ± 0.02	33.9 ± 0.3
10	66.1 ± 0.7	0.59 ± 0.02	34.1 ± 0.3
11	66.1 ± 0.7	0.59 ± 0.02	34.2 ± 0.3
12	66.1 ± 0.7	0.59 ± 0.02	34.2 ± 0.3

Table 5.3: Parameters obtained in the fit of the resolution for the B^0 channel.

Step	μ [fs]	f_1	σ_1 [fs]	f_2
10	-0.82 ± 0.05	0.34 ± 0.02	20.6 ± 0.3	0.071 ± 0.004
11	-0.84 ± 0.05	0.35 ± 0.02	20.6 ± 0.4	0.066 ± 0.004
12	-0.83 ± 0.05	0.35 ± 0.02	20.6 ± 0.4	0.066 ± 0.004
13	-0.83 ± 0.05	0.35 ± 0.02	20.6 ± 0.4	0.066 ± 0.004

Step	σ_2 [fs]	$1 - f_1 - f_2$	σ_3 [fs]
10	67.1 ± 0.8	0.59 ± 0.02	33.9 ± 0.4
11	66.1 ± 0.9	0.59 ± 0.02	33.9 ± 0.4
12	66.1 ± 0.9	0.59 ± 0.02	33.9 ± 0.4
13	66.1 ± 0.9	0.59 ± 0.02	33.9 ± 0.4

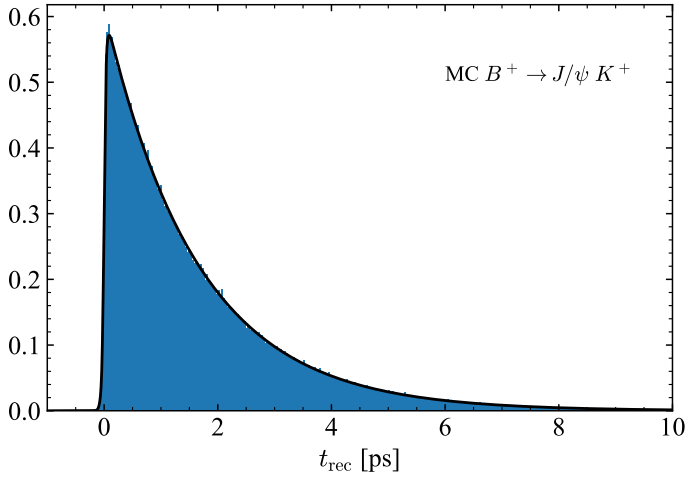

Figure 5.11: In blue, the distribution of reconstructed decay times. In black, the fit of the convolution of a exponential and the sum of three Gaussian distributions.

Once the resolution is obtained, it is convoluted with an exponential distribution to perform the fit for obtaining the lifetime. The result of the convolution of a pure exponential distribution with the sum of three Gaussian distributions with common mean value μ is

$$
\begin{aligned}
f(t) =& \frac{\mathrm{f}_1}{\tau} e^{\frac{1}{2\tau}(2\mu+\frac{\sigma_1^2}{\tau}-2t)} \left(1-\mathrm{erf}\left(\frac{\mu+\frac{\sigma_1^2}{\tau}-t}{\sqrt{2}\sigma_1}\right)\right) \\
&+ \frac{\mathrm{f}_2}{\tau} e^{\frac{1}{2\tau}(2\mu+\frac{\sigma_2^2}{\tau}-2t)} \left(1-\mathrm{erf}\left(\frac{\mu+\frac{\sigma_2^2}{\tau}-t}{\sqrt{2}\sigma_2}\right)\right) \\
&+ \frac{(1-\mathrm{f}_1-\mathrm{f}_2)}{\tau} e^{\frac{1}{2\tau}(2\mu+\frac{\sigma_3^2}{\tau}-2t)} \left(1-\mathrm{erf}\left(\frac{\mu+\frac{\sigma_3^2}{\tau}-t}{\sqrt{2}\sigma_3}\right)\right).
\end{aligned}
$$

The lifetime is obtained by a fit of this function to the distribution of the reconstructed decay time. The fitted function and the distribution are shown in Fig. 5.11.

The results of the lifetime obtained in each step are shown in Fig. 5.12. In these plots it can be observed that the so-called reconstructed lifetime, is in each step 2 fs lower than the ones obtained with true decay times. Nevertheless, they have exactly the same tendency as the true lifetimes.

The candidates present in the fit to the true decay time and the reconstructed decay time are not the same. In order for the fit to the reconstructed decay times to converge, it is necessary to remove some events that have a wrong $t_{\rm rec}$. This is done by requiring the differences between $t_{\rm MC}$ and $t_{\rm rec}$ to be less than 0.46 fs. The

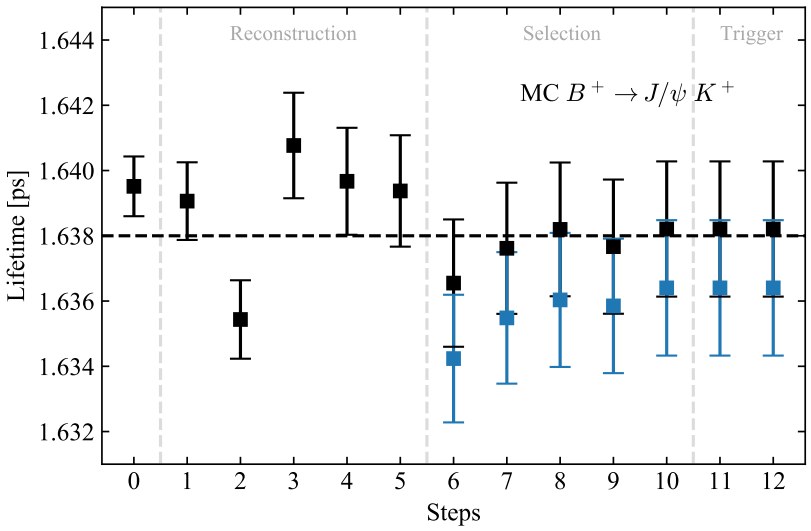

(a)

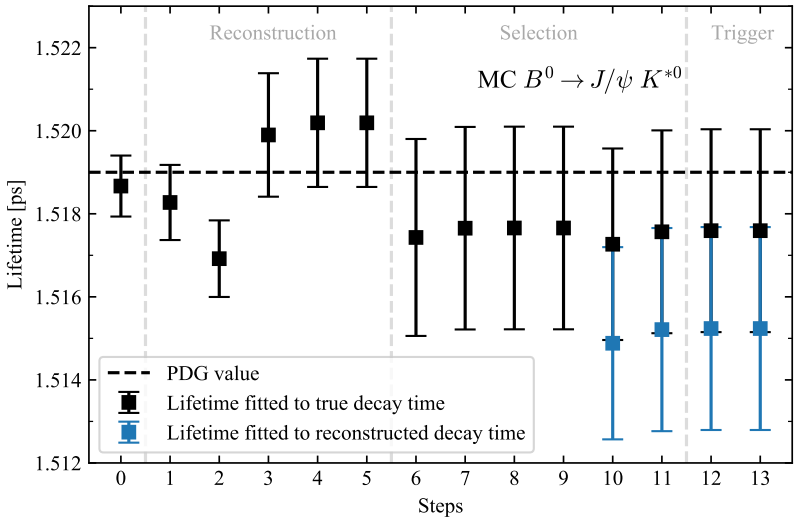

(b)

Figure 5.12: In blue, the lifetime obtained fitting the distribution of reconstructed decay times. In black, the same results as in Fig. 5.3 are shown for comparison.

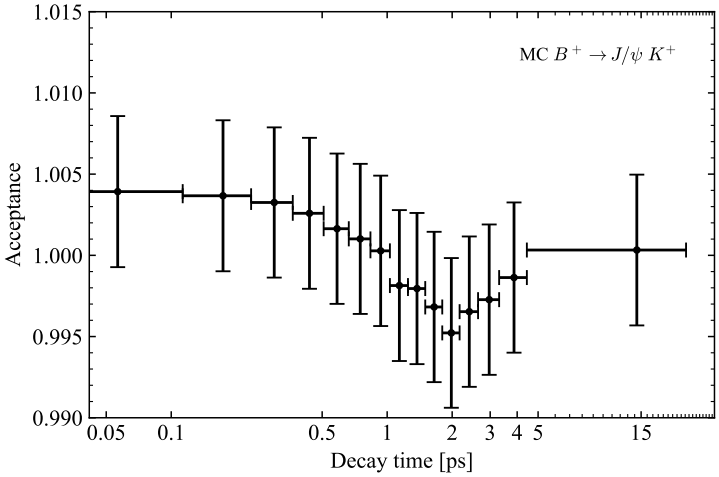

Figure 5.13: Acceptance of the requirement of $|t_{\rm MC} - t_{\rm rec}| < 0.46$ ps necessary for performing the lifetime fit.

acceptance of this requirement is shown in Fig. 5.13. Here, it can be observed a clear dip around 2 ps. There can be multiple reasons that cause the events in that region to have a worse reconstructed decay time value. Unfortunately, due to time constrains this can not be analysed in this thesis. Nevertheless, it is possible to mention some ideas. In a previous measurement of a b meson lifetime [38], a similar acceptance was found when a requirement on the separation between the primary vertex (PV) and b vertex was applied. Events around the 2 ps region had their b meson vertex wrongly reconstructed as an additional PV. This is less likely to happen for very short decay times because their final state tracks are more likely to be used already to obtain the first PV; or to long decay time because the B vertex is at a higher distance from the first PV, where is less likely to reconstruct an additional PV. A similar issue related to the wrong PV can be the cause of the events that have reconstructed decay times distant from the true value.

It is possible to prove that the differences between black and blue points in Fig. 5.12 is due to the requirement of $|t_{\rm MC} - t_{\rm rec}| < 0.46$ ps, necessary for the fit to reconstructed decay times to converge. For that, a fit to the true decay time is performed only using the events that satisfy this requirement. The results are shown in Fig. 5.14. Here one can observe that the results obtained with the decay time from the simulation and with the reconstructed are the same. This plot proves that the model used to obtain the reconstructed decay time, i.e. the evaluation of the resolution and the fit with the convolution to obtain the lifetime is correct. The requirement that is used in this study to be able to perform the fit cannot be done in a lifetime measurement because the true decay time is not known. In the lifetime measurements, it is common to define a region of decay time so that the fit is cleaner,

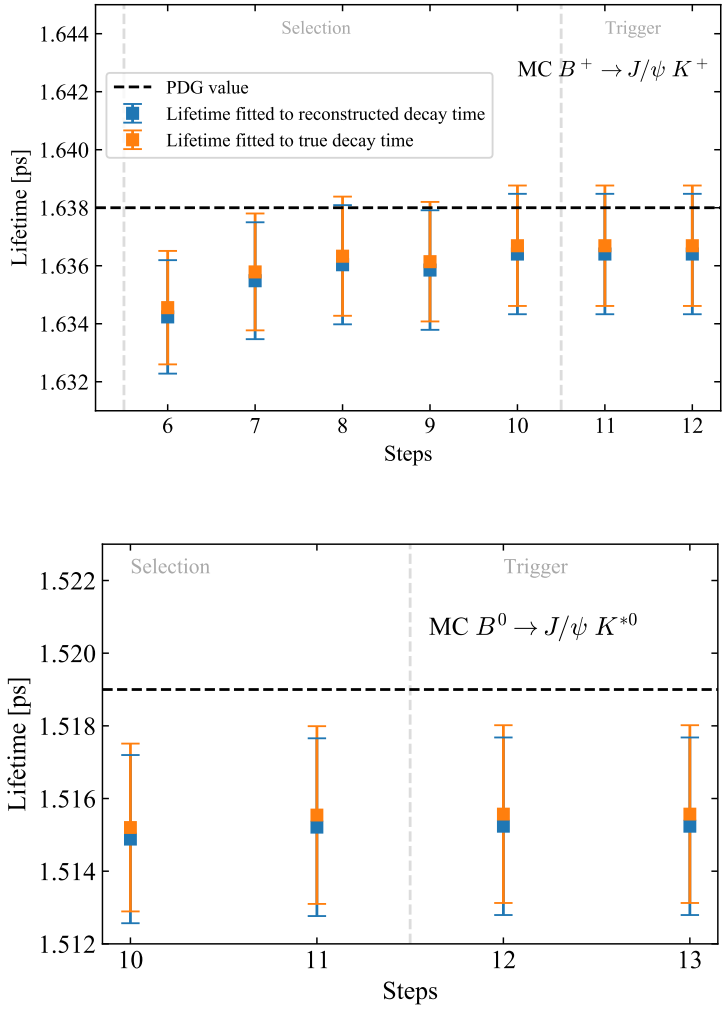

Figure 5.14: Lifetime of the events that satisfy the requirement $|t_{\mathrm{MC}} - t_{\mathrm{rec}}| < 0.46$ ps necessary for performing the lifetime fit.

and then the effects that this might have in the decay time distribution are corrected with the acceptance.

6 Summary

The lifetime bias study presented is part of the evaluation of the physics performance of the LHCb experiment after its upgrade during the second long shutdown LS2. During this period important changes have been introduced in the detector and the trigger strategy in order to prepare for higher luminosity. Therefore, the reconstruction and trigger algorithms have been completely redesigned. To search for possible lifetime bias, the complete data processing has been simulated in MC samples to study its effects in the decay time distributions of the b hadrons. The results obtained serve as preparation for the lifetime and time-dependent measurements that will be carried out with data from Run 3 of LHC.

In the first place, the dependence of the efficiency of each stage of the data processing with the decay time has been studied. For that, different cuts are applied step by step on simulated samples to mimic the reconstruction, the selection, and trigger. After each of these steps, the lifetime is obtained by performing a fit, to study the effects on the true decay time distribution. The study is performed for two decay channels $B^+ \to J/\psi\, K^+$ and $B^0 \to J/\psi\, K^{*0}$ with three and four final state particles respectively. Similar results are obtained in both cases where only a bias of about 3 fs is found, in contrast with the bias of almost 20 fs found in a similar study performed for the Run 1 data. This can be observed in Fig. 6.1 where the lifetimes obtained in each step of data processing are shown.

In the second place, the study focuses on the reconstruction of the b hadrons decay time. For that, the resolution is studied, which indicates the precision of the reconstructed decay time. The resolution obtained in each step of the selection and trigger is reasonable and demonstrates that the calculation of the decay time is correct and is not affected by the data processing. In addition, the reconstructed decay time values are used to obtain the lifetime by a fit similar to those used in real lifetime measurements which includes the resolution. These results are consistent with the ones obtained with the true decay time which validates the model used for the fit and proofs that the distribution of reconstructed decay times is not affected in the data processing.

In conclusion, the results obtained are positive and demonstrate that the new reconstruction framework has a good performance for lifetime and time-dependent measurements.

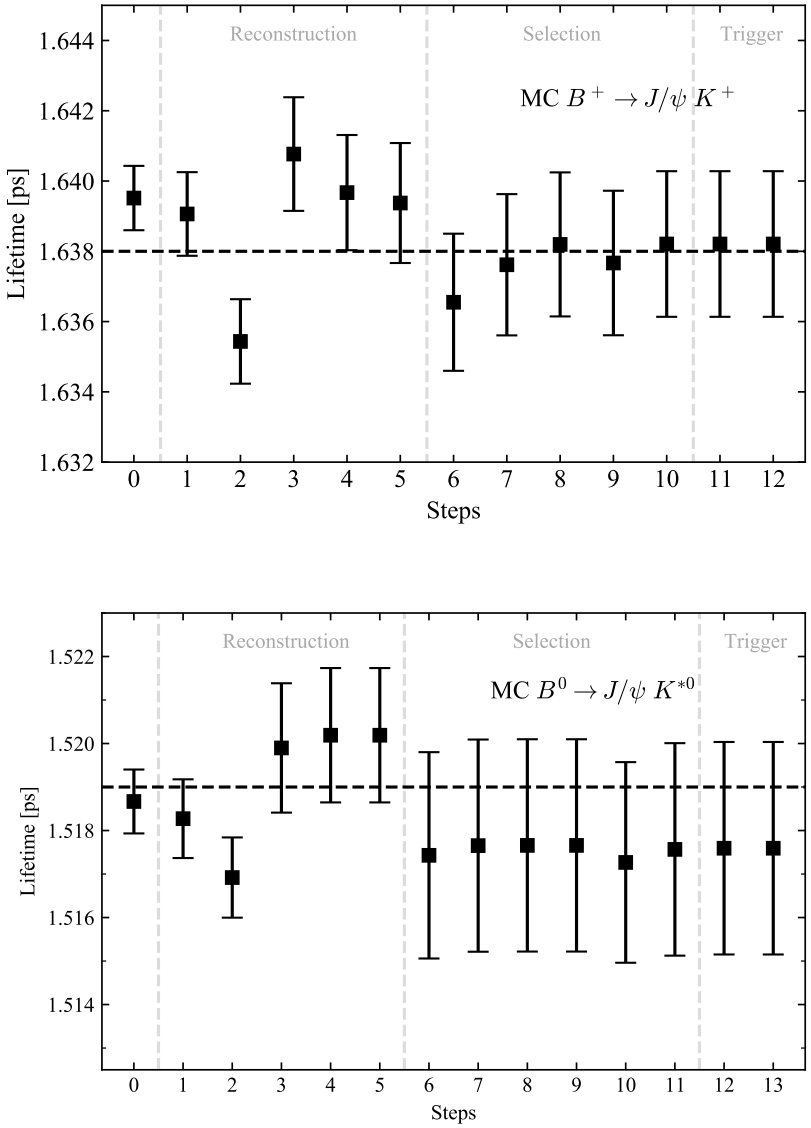

Figure 6.1: Measured lifetime in simulated Monte Carlo samples of $B^+ \to J/\psi\ K^+$ and $B^0 \to J/\psi\ K^{*0}$ after the different requirements of the reconstruction, the selection and the trigger are applied sequentially. The legend of the steps can found in Appendix A. The dashed lines correspond to the average values of the lifetimes of each meson.

6.1 Outlook

Although the results of the study are successful, during the course of this thesis, several technical issues have been faced since the software framework of the LHCb experiment is not completely prepared yet for the analysis of the Run 3 data. This has delayed a lot the processing of the MC samples, necessary to study the performance of the reconstruction algorithms.

This has prevented us from performing the study using a third channel $B_s^0 \to J/\psi\phi$, which has been commonly used for the lifetime measurement of the B_s^0 meson. This is a reasonable option for the improvement of the study. In addition, further analysis of the cause of the wrong calculation of the reconstructed decay time should be carried out.

Nevertheless, the purpose of this study was to evaluate in general the impact of the new reconstruction framework in the time distribution. To take into account the possible small-time bias in future measurement a similar study for the specific data will be performed.

A Steps for the search of lifetime bias

A.1 $B^+ \to J/\psi\ K^+$ decay channel

0. All particles within LHCb geometrical acceptance.
1. Muons $p_{\mathrm{T}} > 550$ MeV/c , kaon $p_{\mathrm{T}} > 1$ GeV/c and $p > 10$ GeV/c.
2. All final state particles tracks are reconstructible as VELO tracks.
3. All final state particles tracks are reconstructible as Long tracks.
4. All final state particles tracks are reconstructed as VELO tracks.
5. All final state particles tracks are reconstructed as Long tracks.
6. Run Moore.
7. $\chi^2_{\mathrm{vtx}}/\mathrm{nDoF}(J/\psi) < 16$, $m(\mu^+\mu^-) \in [3030, 3150]$ MeV/c^2, $\Delta \ln \mathcal{L}_{\mu\pi}(\mu^\pm) > 0$.
8. $\Delta \ln \mathcal{L}_{K\pi}(K^\pm) > 0$.
9. $\chi^2_{\mathrm{IP},B^+} < 25$
10. $\chi^2_{\mathrm{DTF},B^+}/\mathrm{nDoF}(J/\psi) < 5$
11. `HLT1DiMuonHighMass` triggered.
12. `HLT2DiMuonJPsi` triggered.

A.2 $B^0 \to J/\psi\ K^{*0}$ decay channel

0. All particles within LHCb geometrical acceptance.
1. Muons $p_{\mathrm{T}} > 550$ MeV/c , kaon and pion $p_{\mathrm{T}} > 300$ MeV/c.
2. All final state particles tracks are reconstructible as VELO tracks.
3. All final state particles tracks are reconstructible as Long tracks.
4. All final state particles tracks are reconstructed as VELO tracks.
5. All final state particles tracks are reconstructed as Long tracks.

6. Run Moore.
7. $\chi^2_{\text{vtx}}/\text{nDoF}(J/\psi) < 16$, $m(\mu^+\mu^-) \in [3030, 3150]$ MeV/c^2 and $\Delta \ln \mathcal{L}_{\mu\pi}(\mu^\pm) > 0$.
8. $\Delta \ln \mathcal{L}_{K\pi}(K^\pm) > 0$, $\Delta \ln \mathcal{L}_{K\pi}(\pi^\pm) < 0$, $p_{\text{T}}(K^{*0}) > 1.5$ GeV/c and $m(K^+\pi^-) \in [826, 966]$ MeV/c^2.
9. $\chi^2_{\text{vtx}}/\text{nDoF}(K^{*0}) < 16$
10. $\chi^2_{\text{IP},B^+} < 25$
11. $\chi^2_{\text{DTF},B^+}/\text{nDoF}(J/\psi) < 5$
12. `HLT1DiMuonHighMass` triggered.
13. `HLT2DiMuonJPsi` triggered.

B Bibliography

[1] Richard Tilghman Weidner and Laurie M Brown. physics. In *Encyclopedia Britannica*. 2021. URL https://www.britannica.com/science/physics-science.

[2] G. Aad, T. Abajyan, B. Abbott, J. Abdallah, S. Abdel Khalek, A.A. Abdelalim, O. Abdinov, R. Aben, B. Abi, M. Abolins, and et al. Observation of a new particle in the search for the standard model higgs boson with the atlas detector at the lhc. *Physics Letters B*, 716(1):1–29, Sep 2012. ISSN 0370-2693. doi: 10.1016/j.physletb.2012.08.020. URL http://dx.doi.org/10.1016/j.physletb.2012.08.020.

[3] S. Chatrchyan, V. Khachatryan, A.M. Sirunyan, A. Tumasyan, W. Adam, E. Aguilo, T. Bergauer, M. Dragicevic, J. Erö, C. Fabjan, and et al. Observation of a new boson at a mass of 125 gev with the cms experiment at the lhc. *Physics Letters B*, 716(1):30–61, Sep 2012. ISSN 0370-2693. doi: 10.1016/j.physletb.2012.08.021. URL http://dx.doi.org/10.1016/j.physletb.2012.08.021.

[4] LHCb collaboration. Test of lepton universality in beauty-quark decays, 2021.

[5] Roel Aaij et al. Measurement of CP-Averaged Observables in the $B^0 \to K^{*0}\mu^+\mu^-$ Decay. *Phys. Rev. Lett.*, 125(1):011802, 2020. doi: 10.1103/PhysRevLett.125.011802.

[6] Mark Thomson. *Modern Particle Physics*. Cambridge University Press, University Printing House, Cambridge CB2 8BS, United Kingdom, 2013.

[7] R. Kumar. Inclusive decays of B-meson to J/ψ and χ_{c1} using 386×10^6 $B\bar{B}$ events. *Pramana - J Phys .*, 86:471–477, 2016. doi: 10.1007/s12043-015-1166-6. URL https://doi.org/10.1007/s12043-015-1166-6.

[8] LHCb collaboration. Observation of the resonant character of the z(4430)(-) state. *Physical review letters*, 112, 04 2014. doi: 10.1103/PhysRevLett.112.222002.

[9] LHCb Collaboration. "Observation of $J/\psi p$ Resonances Consistent with Pentaquark States in $\Lambda_b^0 \to J/\psi K^- p$ Decays". *Physical Review Letters*, 115 (7), Aug 2015. ISSN 1079-7114. doi: 10.1103/physrevlett.115.072001. URL http://dx.doi.org/10.1103/PhysRevLett.115.072001.

[10] J. H. Christenson, J. W. Cronin, V. L. Fitch, and R. Turlay. Evidence for the 2π decay of the k_2^0 meson. *Phys. Rev. Lett.*, 13:138–140, Jul 1964. doi: 10.1103/PhysRevLett.13.138. URL https://link.aps.org/doi/10.1103/PhysRevLett.13.138.

[11] LHC Guide. Mar 2017. URL http://cds.cern.ch/record/2255762.

[12] LHCb Collaboration. LHCb Tracker Upgrade Technical Design Report. Technical report, Feb 2014. URL https://cds.cern.ch/record/1647400.

[13] P.A. Zyla et al. (Particle Data Group). Review of Particle Physics. *Progress of Theoretical and Experimental Physics*, 2020(8), 08 2020. doi: 10.1093/ptep/ptaa104. URL https://pdg.lbl.gov/2020/reviews/rpp2020-rev-structure-functions.pdf.

[14] LHCb Collaboration. LHCb VELO Upgrade Technical Design Report. Technical report, Nov 2013. URL https://cds.cern.ch/record/1624070.

[15] LHCb Collaboration. *LHCb VELO (VErtex LOcator): Technical Design Report*. Technical design report. LHCb. CERN, Geneva, 2001. URL https://cds.cern.ch/record/504321.

[16] Performance of the LHCb RICH detector at the LHC. *Eur. Phys. J. C*, 73: 2431. 25 p, Nov 2012. doi: 10.1140/epjc/s10052-013-2431-9. URL https://cds.cern.ch/record/1495721.

[17] Massimiliano Fiorini. The upgrade of the lhcb rich detectors. *Nuclear Instruments and Methods in Physics Research Section A: Accelerators, Spectrometers, Detectors and Associated Equipment*, 952:161688, 2020. ISSN 0168-9002. doi: https://doi.org/10.1016/j.nima.2018.12.003. URL https://www.sciencedirect.com/science/article/pii/S0168900218318011. 10th International Workshop on Ring Imaging Cherenkov Detectors (RICH 2018).

[18] Letter of Intent for the LHCb Upgrade. Technical report, CERN, Geneva, Mar 2011. URL https://cds.cern.ch/record/1333091.

[19] CERN (Meyrin) LHCb Collaboration. LHCb Upgrade GPU High Level Trigger Technical Design Report. Technical report, CERN, Geneva, May 2020. URL https://cds.cern.ch/record/2717938.

[20] Peilian Li, Eduardo Rodrigues, and Sascha Stahl. Tracking Definitions and Conventions for Run 3 and Beyond. Technical report, CERN, Geneva, Feb 2021. URL https://cds.cern.ch/record/2752971.

[21] R. Aaij, S. Benson, M. De Cian, A. Dziurda, C. Fitzpatrick, E. Govorkova, O. Lupton, R. Matev, S. Neubert, A. Pearce, H. Schreiner, S. Stahl, and

M. Vesterinen. A comprehensive real-time analysis model at the lhcb experiment. *Journal of Instrumentation*, 14(04):P04006–P04006, Apr 2019. ISSN 1748-0221. doi: 10.1088/1748-0221/14/04/p04006. URL http://dx.doi.org/10.1088/1748-0221/14/04/P04006.

[22] CERN (Meyrin) LHCb Collaboration. Computing Model of the Upgrade LHCb experiment. Technical report, CERN, Geneva, May 2018. URL https://cds.cern.ch/record/2319756.

[23] M Clemencic et al. The LHCb simulation application, gauss: Design, evolution and experience. *Journal of Physics: Conference Series*, 331(3):032023, dec 2011. doi: 10.1088/1742-6596/331/3/032023. URL https://doi.org/10.1088/1742-6596/331/3/032023.

[24] Torbjörn Sjöstrand et al. An introduction to pythia 8.2. *Computer Physics Communications*, 191:159–177, 2015. ISSN 0010-4655. doi: https://doi.org/10.1016/j.cpc.2015.01.024. URL https://www.sciencedirect.com/science/article/pii/S0010465515000442.

[25] David J. Lange. The evtgen particle decay simulation package. *Nuclear Instruments and Methods in Physics Research Section A: Accelerators, Spectrometers, Detectors and Associated Equipment*, 462(1):152–155, 2001. ISSN 0168-9002. doi: https://doi.org/10.1016/S0168-9002(01)00089-4. URL https://www.sciencedirect.com/science/article/pii/S0168900201000894. BEAUTY2000, Proceedings of the 7th Int. Conf. on B-Physics at Hadron Machines.

[26] S. Agostinelli et al. Geant4—a simulation toolkit. *Nuclear Instruments and Methods in Physics Research Section A: Accelerators, Spectrometers, Detectors and Associated Equipment*, 506(3):250–303, 2003. ISSN 0168-9002. doi: https://doi.org/10.1016/S0168-9002(03)01368-8. URL https://www.sciencedirect.com/science/article/pii/S0168900203013688.

[27] Alexander Lenz. Lifetimes and hqe, 2019.

[28] LHCb Collaboration. Precision measurement of the Λ_c^+, Ξ_c^+ and Ξ_c^0 baryon lifetimes. *Phys. Rev. D*, 100:032001. 12 p, Jun 2019. doi: 10.1103/PhysRevD.100.032001. URL https://cds.cern.ch/record/2683283. 9 pages, 2 figures. All figures and tables, along with any supplementary material and additional information, are available at https://cern.ch/lhcbproject/Publications/p/LHCb-PAPER-2019-008.html.

[29] Roel Aaij et al. Measurement of the Ω_c^0 baryon lifetime. *Phys. Rev. Lett.*, 121 (9):092003, 2018. doi: 10.1103/PhysRevLett.121.092003.

[30] M. Kirk, A. Lenz, and T. Rauh. Dimension-six matrix elements for meson mixing and lifetimes from sum rules. *Journal of High Energy Physics*, 2017

(12), Dec 2017. ISSN 1029-8479. doi: 10.1007/jhep12(2017)068. URL http://dx.doi.org/10.1007/JHEP12(2017)068.

[31] LHCb Collaboration. Precise determination of the B_s^0-$\overline{B}_s^0$ oscillation frequency. Precise determination of the $B_s^0 - \bar{B}_s^0$ oscillation frequency. Technical report, CERN, Geneva, Apr 2021. URL http://cds.cern.ch/record/2764338. All figures and tables, along with any supplementary material and additional information, are available at https://cern.ch/lhcbproject/Publications/p/LHCb-PAPER-2021-005.html (LHCb public pages).

[32] Francesca Dordei. *Lifetime measurements of beauty hadrons at the LHCb experiment*. PhD thesis, Ruperto-Carola-University of Heidelberg, 5 2015.

[33] F. James. *MINUIT Function Minimization and Error Analysis*. CERN Computing and Networks Division, 1994.

[34] P. A. Zyla et al. Review of Particle Physics. *PTEP*, 2020(8):083C01, 2020. doi: 10.1093/ptep/ptaa104.

[35] Y. Amhis, Sw. Banerjee, E. Ben-Haim, F. U. Bernlochner, M. Bona, A. Bozek, C. Bozzi, J. Brodzicka, M. Chrzaszcz, J. Dingfelder, and et al. Averages of b-hadron, c-hadron, and τ-lepton properties as of 2018. *The European Physical Journal C*, 81(3), Mar 2021. ISSN 1434-6052. doi: 10.1140/epjc/s10052-020-8156-7. URL http://dx.doi.org/10.1140/epjc/s10052-020-8156-7.

[36] A. Hennequin, B. Couturier, V.V. Gligorov, S. Ponce, R. Quagliani, and L. Lacassagne. A fast and efficient simd track reconstruction algorithm for the lhcb upgrade 1 velo-pix detector. *Journal of Instrumentation*, 15(06): P06018–P06018, Jun 2020. ISSN 1748-0221. doi: 10.1088/1748-0221/15/06/p06018. URL http://dx.doi.org/10.1088/1748-0221/15/06/P06018.

[37] CERN The LHCb Collaboration. Upgrade Software and Computing. Technical report, CERN, Geneva, Mar 2018. URL https://cds.cern.ch/record/2310827.

[38] Simon Stemmle. *CP violation and lifetime measurements in the decay $B_s^0 \to J/\psi\phi$ with the LHCb experiment*. PhD thesis, Ruperto-Carola-University of Heidelberg, 7 2019.

Erklärung:

Ich versichere, dass ich diese Arbeit selbstständig verfasst habe und keine anderen als die angegebenen Quellen und Hilfsmittel benutzt habe.

Heidelberg, den (Datum) .....